Monatshefte für Chemie 128, 443–474 (1997)

*Monatshefte für Chemie*
*Chemical Monthly*


# Molecular Mechanical and Quantum Chemical Study of the Species Involved in the Hydrolysis of *cis*-Diamminedichloroplatinum(II) and Substituted *Bis*(ethylenediamine)-dichloroplatinum(II) Complexes II. Simulated Transition States

**G. S. Nikolov[1,*], N. Trendafilova[1], I. Georgieva[1], H. Schönenberger[2], R. Gust[2], J. Kritzenberger[3], and H. Yersin[3]**

[1] Institute of General and Inorganic Chemistry, Bulgarian Academy of Sciences, BG-1113 Sofia, Bulgaria and Department of Physical and Theoretical Chemistry, University of Plovdiv, BG-4000 Plovdiv, Bulgaria
[2] Institute of Pharmacy, University of Regensburg, D-93040 Regensburg, Germany
[3] Institute of Physical and Theoretical Chemistry, University of Regensburg, D-93040 Regensburg, Germany

**Summary.** *cis*-Diamminedichloroplatinum(II) (cisplatin) and its substituted ethylenediamine derivatives *cis*-$PtCl_2(R_2en)$ (*en* = ethylenediamine, *R* = H, Ph, 2-, 3-, and 4-PhOH) have been investigated with respect to the possible structures of the hypothetical Transition State Complexes (*TSC*) of the hydrolytic $S_N2$ reaction in which one Cl is replaced by $H_2O$. *TSC*s with *trigonal bipyramid* (*TBP*) and *square pyramid* (*SP*) geometry (coordination number 5), have been studied by Molecular Mechanics (*MM*) and Extended *Hückel* (*EH*) methods. The *EH* and *MM* energies as well as the number of occurrence (entropy factor) for the cisplatinum compound point to a preferred *TBP TSC* geometry with $NH_3$ and Cl in axial positions. However, for *en* and substituted *en* compounds, *TSC*s with *SP* geometries (Cl in apical position) are preferred. The calculated *EH* and *MM* energies of the *TBP* and *SP* structures do not differ significantly and *TBP* ↔ *SP* interconversions may play an essential role in *TSC* formation. To improve the discrimination, the *MM*-optimized geometries were treated in terms of displacement coordinates for $D_{3h}$ (*TBP*) and $C_{4v}$ (*SP*) by calculating the total distortion vectors (*DV*). *DV* identified once again the *TBP* with $NH_3$ and Cl in axial position as the least-distorted conformer, but it also revealed the combinations of displacement coordinates which shape the *TSC* geometry.

**Keywords.** Platinum coordination compounds; Antitumor activity; Molecular modelling.

**Molekularmechanische und quantenchemische Untersuchung der bei der Hydrolyse von *cis*-Diammindichlorplatin(II) und substituierten *Bis*(ethylendiamin)dichlorplatin(II)-Komplexen auftretenden Spezies, 2. Mitt. Simulierte Übergangszustände**

**Zusammenfassung.** *cis*-Diammindichlorplatin(II) (Cisplatin) und seine substituierten Ethylendiaminderivate *cis*-$PtCl_2(R_2en)$ (*en*=Ethylendiamin, $R = H$, Ph, 2-, 3- und 4-PhOH) wurden im Hinblick auf mögliche Strukturen der hypothetischen Übergangszustandkomplexe (*TSC*) der hydrolytische $S_N2$-Reaktion (Substitution eines Cl-Atoms durch $H_2O$) untersucht. *TSC*s mit trigonal-bipyramidalen (*TBP*) und quadratisch-pyramidalen (*SP*) Geometrien (Koordinationszahl 5) wurden mit molekularmechanischen (*MM*) und Extended-*Hückel*-Methoden (*EH*) behandelt. *EH*- und *MM*-Energien sowie entropische Faktoren weisen für Cisplatin auf eine trigonale Bipyramide mit $NH_3$ und Cl in axialen Positionen als bevorzugte *TSC*-Geometrie hin, während für Komplexe mit *en*-Liganden *SP*-Geometrien mit Cl in der apicalen Position energetisch begünstigt sind. Da die berechneten *EH*- und *MM*- Energien für *TBP*- und *SP*-Geometrien sehr ähnlich sind, spielen möglicherweise *TBP-SP*-Umwandlungen eine wesentliche Rolle bei der Bildung der *TSC*s. Zur Verbesserung der Unterscheidung wurden für die *MM*-optimierten Geometrien die Verschiebungsvektoren (*DV*) bezüglich $D_{3h}$ (*TBP*) und $C_{4v}$ (*SP*) berechnet. Daraus resultierte erneut die trigonale Bipyramide mit $NH_3$ und Cl in den axialen Positionen als das am wenigsten gespannte Konformere; des weiteren konnten mit dieser Methode die Kombinationen der Verschiebungskoordinaten erhalten werden, die für die Ausbildung der *TSC*-Geometrie verantwortlich sind.

## Introduction

It is generally believed that the first stage of the physiological action of the cisplatin complexes as cytostatic reagents is their hydrolysis [2, 3] in which one $Cl^-$ is replaced by a $H_2O$ molecule. This is the rate-determining stage prior to the platinum complex penetration into the cell. In part I of this investigation [1] we have studied the possible geometries of the reactants and the products of this hydrolytic reaction for a number of Pt(II) compounds with ethylenediamine (**1**-$PtCl_2$) and its derivatives: **2**-$PtCl_2$, **3**-$PtCl_2$, **4**-$PtCl_2$, and **5**-$PtCl_2$ (Fig. 1). These compounds have been tested against cancer cell lines as tumor models [4–8]. In Ref. [1], the thermodynamic stability was shown to be correlated with the rate of hydrolysis of *meso (R,S)*- and *d,l* (*R,R/S,S*)-[1,2-*bis*(2-hydroxyphenyl)ethylenediamine] dichloroplatinum(II) (**3**-$PtCl_2$). The slower rate of hydrolysis of the (*R,S)* diastereoisomer as compared with that of the (*R,R/S, S*) species of **3**-$PtCl_2$ was

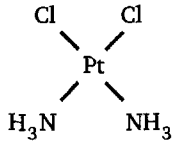


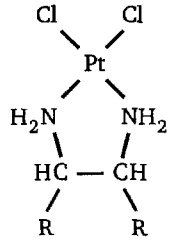


cisplatin

| *R* | Compound |
|---|---|
| H | 1-$PtCl_2$ |
| Ph | *meso–, d,l–* 2-$PtCl_2$ |
| 2-OH-Ph | *meso–, d,l–* 3-$PtCl_2$ |
| 3-OH-Ph | *meso–, d,l–* 4-$PtCl_2$ |
| 4-OH-Ph | *meso–, d,l–* 5-$PtCl_2$ |

**Fig. 1.** Structural diagrams of cisplatin (a) and related compounds (b); *meso* = (*R,S*), *d,l* = (*R,R/S,S*)

explained by the presence of a 5th Pt-O contact in the (*R, S*) diastereoisomer which blocks one position in the planar complex and thus hinders the entrance of the water molecule.

The present study reports on the possible structures of the Transition State Complexes (*TSC*) for the hydrolytic reaction in an attempt to identify the lowest-energy $S_N2$ mechanistic pathways. The two highest-symmetry 5-coordinate $ML_5$ species are *square planar (SP)* and *trigonal bipyramidal* (*TBP*) arrangements [9, 10]. Since the *TSC*s are not accessible experimentally and a selection in advance cannot be made in our theoretical studies, we consider both the *TBP* and *SP* structures and all possible conformers.

The approach used in this work is as follows: we construct all possible geometric isomers for an *SP* or *TBP* [Pt(*L-L*)$Cl_2(H_2O)$] *TSC* and optimize the structures by Molecular Mechanics (*MM*) calculations. This is in fact a grid search in the *SP* and *TBP* spaces. Some isomers were found to retain the initial (input) ligand arrangement; however, others changed the initial locations of the ligands to produce a new (distorted) arrangement or another isomer. By comparing the *MM* (strain) energies, the preferred pathways were discerned; further, by counting the number of occurrence of the isomers as final structures, we were in a position to access also the entropy factor characterizing the pathway. Extended *Hückel* (*EH*) calculations with *MM*-optimized geometries were used to provide the basis of assessing the relative electronic factor stability order of the *TSC* structures. *Ab initio* calculations for such large species are practically impossible. Since both *MM* and *EH* results gave energy values close to each other and therefore do not help much discriminate the different *TSC* geometries, an attempt was made to classify these geometries in terms of displacement coordinates.

## Methods

*MM* was developed as the main tool for conformational transition state studies in organic chemistry [11]. Because of the presence of d-AO and the action of 1st and 2nd order *Jahn-Teller* effects, *MM* applications to inorganic compounds were subject to some criticism [12, 13]. However, at present there are numerous examples which show that *MM* can be used reliably to attact conformational problems also in inorganic chemistry [14, 14a]. In some cases, the *MM* results were better than those from *ab initio* [15] and semiempirical (AM1, combined *QM/MM*) methods [13]. *MM* of Pt compounds has been shown to be highly successful in Ref. [16], and our results from Ref. [1] provide solid evidence to this claim reproducing the cystallographic data (bond lengths, valence angles) for the studied reactants. Proof that molecular mechanics can be used to study *TSC* is given in Refs. [16–21].

The standard *MMX* method [17], employed both in Ref. [1] and in the present investigation, uses the strain energy to decide which *TSC* is the most stable one. *MMX,* based on *MM2,* uses the standard *Hook*'s expressions for stretch, bend, and cross term interactions; it also includes *van der Waals* and dipole-dipole interactions. Parameters used in our calculations are given in the appendix and comprise the standard set used in *MMX*. For the sake of comparison, *MM* parameters used by other researchers are also given there. The differences are minor. *LML* interactions as stated in Ref. [14] are neglected ($k = 0.0\,\mathrm{mdyn \cdot \AA^{-1}}$), but ligand-to-ligand repulsion is explicitly accounted for by the *van der Waals* and dipole-dipole interactions. The problem of treating the *L*Pt*L* angles, which differ in *SP* and *TBP*, was handled by 1–3 non-bonded interactions as suggested elsewhere [14a, 16c]. This allows Pt(II) to adopt the coordination geometry most favourable to the *TSC,* not limiting it to an *a*

*priori* geometry [14d]. Thus, only bonding parameters for each type of new geometry need to be derived. There is ample evidence that the same set of bonding parameters can be used to treat different geometries; in Ref. [16], Pt-N in the *TSC* had been made only 0.05 Å longer without any further modification in the force field.

The extended *Hückel* calculations were performed employing a version which uses a metal-ligand distance dependent formula to calculate the off-diagonal elements and the geometry parameters from the *MM* calculations [22]. Charge iteration was performed in all cases. The atom parameters were taken basically from the collections of *Fitzpatrick* and *Murphy* [23], but the Pt orbital exponent had to be readjusted back to a *Slater* type orbital (*STO*) in order to obtain a slightly positive Pt charge in the complex; with *Fitzpatrick*'s parameters, $q$(Pt) was always negative. The shifts in $q$(Pt) values are interpreted only in a comparative manner, their absolute values being not essential. The Pt valence state ionization parameters (*VSIP*) were taken from Ref. [24]. Three different energies were obtained by the *EH* method: sum of orbital energies, orbital stabilization energy (*OS*), and repulsion energy. In order to facilitate comparison between differently constituted complexes, we used the orbital stabilization energy which is defined as the difference between the sum of energies for the orbitals populated with electrons and the respective *VSIP* [22]. This energy was termed as *EH,* and it provides the energy lowering produced from the constituent Pt(II) and ligands taken in their standard states. The procedure of describing molecular geometries in terms of displacement symmetry coordinates using a total distortion vector is given in Ref. [25]. The symmetry-adapted linear combinations of the displacement coordinates for $D_{3h}$ and $C_{4v}$ were given also in Ref. [25]. We have used them to calculate the distortion vectors (*DV*) in the *TBP* and *SP* spaces. Our *DV*s, unlike the procedure adopted in Ref. [25], include all (stretch and bend) coordinates with the increments relative to the reference *TBP* or *SP* species taken from *MM*. The *DV* is defined as

$$D = \sum_{j} \Delta d_j p_j = \sum_{j} (d_j(\text{calc}) - d_j(\text{ref}))p_j$$

where $d_j$(calc) and $d_j$(ref) represent either the bond lengths or the valence angles of the calculated and reference molecules, respectively; the sum is taken over all 12 coordinates $p_j$. $\Delta d_j$ reflects the *TSC* displacement along the coordinate $p_j$ away from the reference *TBP* or *SP* structure. The coordinates obtained represent two new coordinate systems (spaces) in which each *TSC* geometry could be represented by a point given by the magnitudes of the displacement along the respective coordinate (for details, see Ref. [25]). These two spaces have been called *TBP* and *SP* space.

The valence angles used in our study for the *TBP* and *SP* reference structures are in agreement with those given in Ref. [25]. The reference Pt-Cl and Pt-N bond lengths of our *TSC* structures were standard for five coordinate metal complexes [25]: Pt-Cl = 2.497 Å, Pt-N = 2.221 Å, and Pt-O- = 1.97 Å. They differ from the standard bond lengths in *MMX* (2.300, 1.980, and 1.800 Å, respectively), but they are close (*vide infra*) to the bond length values of the *MM*-optimized structures (2.40, 1.96, and 2.12 Å, respectively).

## Results and Discussion

### *A. MM and EH Calculations*

#### 1. Geometry Isomers

The transition state complex that may be formed upon nucleophilic addition of a water molecule to a cisplatin complex or its derivatives is

$$[\text{Pt}(L\text{-}L)\text{Cl}_2] + \text{H}_2\text{O} = [\text{Pt}(L\text{-}L)(\text{H}_2\text{O})\text{ClCl}]^{\#} \qquad (1)$$

where *L-L* stands for two $NH_3$, or one ethylenediamine (*en*) or substituted *en,* as given in Fig. 1.

**Table 1.** Energy data (*MM*[a] and *EH*[a]) and charge distribution in the transition state complexes

| Transition state complex | Structures | | | | | | | | |
|---|---|---|---|---|---|---|---|---|---|
| $Pt(NH_3)_2Cl_2(H_2O)$ | ($a_1$) *SP* $O_{ap}$ | ($a_3$) *TBP* $NO_{ax}$ | ($a_4$) *TBP* $NO_{ax}$ | (b) *TBP* $NO_{ax}$ | (d) *TBP* $NN_{ax}$ | (e) *TBP* $NN_{ax}$ | ($a_2$) *TBP* $NN_{ax}$ | (f) *TBP* $NCl_{ax}$ | (c) *TBP* $NCl_{ax}$ |
| *EH* (eV) | −72.09 | −71.68 | −71.94 | −71.80 | −71.38 | −71.89 | −71.37 | −71.80 | −71.65 |
| *q*(Pt) | 0.052 | 0.052 | 0.052 | 0.053 | 0.042 | 0.047 | 0.042 | 0.053 | 0.052 |
| *q*(Cl) | −0.58 | −0.63 | −0.65 | −0.58 | −0.62 | −0.63 | −0.63 | −0.60 | −0.56 |
| *MM* (kcal·mol$^{-1}$) | 8.1 | 8.0 | 8.0 | 8.0 | 7.7 | 7.7 | 7.5 | 8.0 | 8.0 |
| *TBP trans*-axial (*SP* basal) angles (°) | 164 151 | 173 | 173 | 171 | 176 | 175 | 176 | 175 | 172 |
| **1**-$PtCl_2$ ($H_2O$) | ($a_1$) = (c) *SP*[b] $O_{ap}$ | | ($a_2$) *SP*[b] $N_{ap}$ | ($a_3$) *SP*[b] $N_{ap}$ | | (b) *SP*[b] $Cl_{ap}$ | (f) *SP*[b] $Cl_{ap}$ | (d) *SP*[b] $Cl_{ap}$ | (e) *SP*[b] $Cl_{ap}$ |
| *EH* (eV) | −102.02 | | −101.61 | −101.44 | | −101.76 | −101.76 | −101.74 | −101.74 |
| *q*(Pt) | 0.046 | | 0.062 | 0.07 | | 0.045 | 0.045 | 0.042 | 0.042 |
| *q*(Cl) | −0.58 | | −0.56 | −0.56 | | −0.58 | −0.65 | −0.65 | −0.66 |
| *MM* (kcal·mol$^{-1}$) | 7.3 | | 7.8 | 7.8 | | 7.5 | 7.5 | 7.3 | 7.3 |
| *trans*-basal (*SP*) angles (°) | 166 157 | | 173 159 | 176 174 | | 159 158 | 159 158 | 168 131 | 165 146 |
| **2**-$PtCl_2$ ($H_2O$) | ($a_1$) *SP*[b] $O_{ap}$ | | ($a_2$) *SP*[b] $N_{ap}$ | ($a_3$) *SP*[b] $N_{ap}$ | | ($a_4$) = (b) = (c) *SP*[b] $Cl_{ap}$ | | | (d) = (e) *SP*[b] $Cl_{ap}$ |
| *EH* (eV) | −270.20 | | −269.63 | −269.67 | | −269.55 | | | −270.08 |
| *q*(Pt) | 0.044 | | 0.061 | 0.066 | | 0.037 | | | 0.042 |
| *q*(Cl) | −0.56 | | −0.56 | −0.56 | | −0.64 | | | −0.65 |
| *MM* (kcal·mol$^{-1}$) | 24.8 | | 25.9 | 26.9 | | 24.3 | | | 24.5 |
| *trans*-basal (*SP*) angles (°) | 161 163 | | 172 158 | 174 171 | | 159 155 | | | 159 156 |
| **3**-$PtCl_2$ ($H_2O$) | ($a_1$) *SP*[b] $O_{ap}$ | | (b) = (c) = (d) *SP*[b] $N_{ap}$ | ($a_2$) *SP*[b] $N_{ap}$ | | ($a_3$) *SP*[b] $N_{ap}$ | | | ($a_4$) = (e) *SP*[b] $Cl_{ap}$ |
| *EH* (eV) | −279.52 | | −279.40 | −279.42 | | −279.40 | | | −279.49 |
| *q*(Pt) | 0.040 | | 0.050 | 0.060 | | 0.064 | | | 0.041 |
| *q*(Cl) | −0.58 | | −0.57 | −0.56 | | −0.57 | | | −0.65 |
| *MM* (kcal·mol$^{-1}$) | 22.6 | | 23.0 | 23.2 | | 24.0 | | | 23.1 |
| *trans*-basal (*SP*) angles (°) | 168 155 | | 172 142 | 173 157 | | 172 168 | | | 160 154 |

[a] *MM:* Molecular Mechanics *EH:* Extended *Hückel* (orbital stabilization) energies;
[b] *gauche* forms (*S,S*), ax axial, ap apical

The *EH* (orbital stabilization) and *MM* (strain) energies obtained as well as some geometry parameters of the simulated *TSC* are listed in Table 1. We shall discuss the energy values separately for the differently constituted compounds. The geometry parameters will receive special attention in *Section B.*

### $[Pt(NH_3)_2Cl_2(H_2O)]$

Figure 2 illustrates the *MM* results for this species. The first row reflects the starting structures which were chosen as input in the *MM* optimization as physically discernible geometric isomers. The second row depicts the geometries resulting from the *MM* optimization as output which are further used in the *EH* calculations.

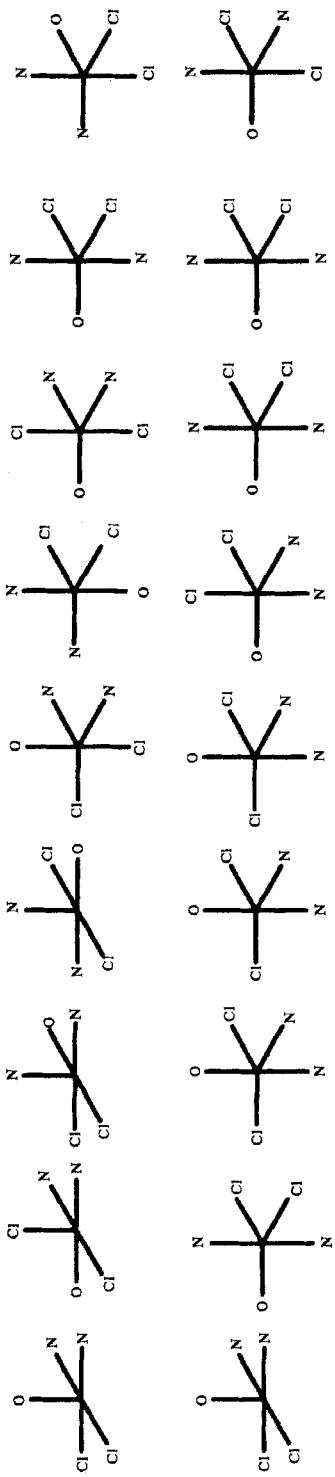


**Fig. 2.** Start (first row) and optimized (second row) geometries of transition state complexes for $Pt(NH_3)_2Cl_2(H_2O)$; the letters (a)–(f) are used in Table 1 to denote the structures

It should be noted that all optimized structures are intermediates between *SP* and *TBP*. However, they are termed either as *SP* or *TBP* based on the values of the valence angles using the following guidelines: *SP* shows two angles that are equal or close to 180° (these are the two *trans*-basal angles), whereas *TBP* shows only one angle that is equal or close to 180°, the remaining angles being either close to 120° (equatorial) or 90° (meridional). There is a much better procedure of describing the deviations from the two ideal structures which will be discussed in detail in *Section B*.

Not all geometry isomers used as starting structures were obtained as local minima. This means that some input isomers were lacking as output structures. From the five possible arrangements of the five ligands at the *TBP*'s *trans*-axial sites, only three distinct isomers with axial ligand pairs $NH_3$-$H_2O$, $NH_3$-Cl, and $NH_3$-$NH_3$ were obtained as output structures. The Cl-Cl and Cl-$H_2O$ pairs in *trans*-axial positions could not be obtained as *MM*-optimized structures. The starting structures with $NH_3$-$NH_3$ and $NH_3$-Cl in *trans*-axial positions were retained in the *MM* minimization procedure. However, the structures with $NH_3$-$H_2O$, Cl-Cl, and Cl-$H_2O$ in axial positions exchange axial with equatorial ligands or *vice versa* during the *MM* minimization process. Hence, $NH_3$-$H_2O$ is not retained but produced from *trans* Cl-$H_2O$ *TBP* and some *SP* starting structures.

Several conclusions can be drawn from Fig. 2:

(*i*) Out of 4 *SP* and 5 *TBP* distinct starting structures we obtained 8 *TBP* and 1 *SP*. The only *SP* has $H_2O$ in the apical position. The 8 *TBP* are $NH_3$-$NH_3$ in *trans*-axial positions (3), $NH_3$-$H_2O$ (3), and $NH_3$-Cl (2); the numbers in parentheses are the numbers of structures with equal geometries obtained from different starting structures. These numbers will be called numbers of occurrence and will be used to assess the entropy factor. In fact, all these numbers should be multiplied by a factor of four since there are two pairs (N, N and Cl, Cl) of undistinguishable atoms.

One axial position is always occupied by $NH_3$; the second axial positon is taken by $NH_3 \sim H_2O > Cl$ in the order of decreasing frequency of occurrence, $NH_3$ and $H_2O$ being more likely to occur than Cl. These numbers of occurrence are important since they give the entropy contributions to the reaction rate constant [26]. Since entropy is the measure for the number of ways of realizing an object [26], the entropy contribution is highest for the highest number of occurrence. From the entropy point of view, the most probable *TBP TSC* structures are those with *trans*-axial $NH_3$-$NH_3$ and $NH_3$-$H_2O$. For *en* and substituted *en* complexes, however, the *trans* $NH_3$-$NH_3$ species should be discarded (*vide infra*).

The species resulting from aquation of $[Pt(NH_3)_2Cl_2]$ form the following series:

| *trans*-axial | *TBP* (N-N) | | *TBP* (N-Cl) | | *TBP* (N-O) | | *SP* (O apical) |
|---|---|---|---|---|---|---|---|
| *MM* | 7.6 | < | 8.0 | ~ | 8.0 | < | 8.1 kcal · mol$^{-1}$ |
| *EH* | −71.5 | ~ | −71.7 | ~ | −71.8 | > | −72.1 eV |

It can be seen that both the *MM* and *EH* energies vary very modestly in this series (~ 0.5 kcal · mol$^{-1}$ for *MM* and 0.6 eV for *EH* within exp. error). Hence, it is highly desirable to find a better descriptor of the studied structures (*vide infra*).

(*ii*) The most stable (lowest energy) 5-coordinate *TSC* is the *trans*-axial $NH_3$-$NH_3$ species resulting from 3 different starting geometries (cases (d), (e), and

($a_2$) in Fig. 2 and Table 1). It shows the lowest *MM* energy (7.5 and 7.7 kcal · mol$^{-1}$) and lowest positive charges on Pt, which would facilitate the release of the negative $Cl^-$ anion during the *TSC* decomposition to the hydrolysis product.

The $NH_3$-$NH_3$ structures (d) = (e) are a compressed *TBP* with Pt-N = 2.12 Å (axial), Pt-Cl = 2.4 Å, and Pt-$OH_2$ = 1.96 Å (equatorial). These values are in agreement with other *MO* calculations [10b]. The structures can also be termed as bisphenoid $C_{2v}$ with Pt-O on the $C_2$ axis (Table 1). The equatorial Pt-Cl bonds are in fact the same (2.44 Å) as those in the reactant (Pt-Cl = 2.43 Å, exp. value 2.33 Å, see Ref. [1]). The $NH_3$-$NH_3$ structure does not favour the *trans*-effect manifestation of the strong $\sigma$-donor ($NH_3$) ligands, since both $NH_3$ ligands are in *trans*-axial position [10b]. Hence, despite the low positive charge on Pt and the low *MM* energy, it is expected that the mechanistic path for the hydrolysis reaction *via* the *trans*-axial $NH_3$-$NH_3$ *TSC* would be unfavourable.

Second in *MM* energy are the structures with *trans*-axial $NH_3$-Cl ((c), (f)) and $NH_3$-$H_2O$ (($a_3$), ($a_4$) (b)) which have equal *MM* and close *EH* energies. They are by 0.4 kcal · mol$^{-1}$ higher in *MM* energy (within calc. error) and 0.2 eV in *EH* energy than the *trans*-axial $NH_3$-$NH_3$ structure. Although the Pt-Cl distances are equal in both forms and the $q$(Pt) are more positive in the *trans*-axial $NH_3$-Cl *TSC* than in the $NH_3$-$NH_3$ *TSC*, due to the small difference in *MM* energy and the expected labilizing effect of equatorial $NH_3$, this species offers better conditions for the hydrolysis of the cisplatinum complex.

### *Pt(en)Cl$_2$(H$_2$O)* (**1**-$PtCl_2(H_2O)$)

When two $NH_3$ are substituted by one *en* ligand, regardless of the input geometry, the resulting *TSC* geometry is exclusively an *SP* intermediate (Fig. 3). The number of possible starting geometries as compared with cisplatin is reduced because *en* can coordinate only in neighbouring positions. The donor atoms O, Cl, and N can occupy the apical position.

The *TSC* structures resulting after *MM* energy minimization can be classified with respect to their number of occurrence as follows: 4 with Cl at apical position ((b) = (f), (e = d)), 2 with N at the apical position (($a_2$), ($a_3$)), and 2 with O at the apical position (($a_1$) = (c)), (see Table 1). Hence, the most probable structure has apical Cl. It seems that *en* prefers the basal sites in *SP* (see also Ref. [10b]). Conversely, by taking up one basal site and the apical position, the bite angle of *en* would have to be larger than 90°, which is quite uncommon for *bis* bidentate *en* complexes (usually ~80°) [9, 27]. The opening of NPtN, accompanied by reduced repulsion in the basal plane, increases the strain energy in the coordinated *en*. Two structures ((e) = (d)) deviate from *SP* on the way to *TBP* (see *trans*-basal angles in Table 1) more strongly than the other two ((b) and (f)). It should be also noted that the *en* ligand cannot occupy the equatorial position in a *TBP* since its bite angle NPtN would have to be ~120°, much higher than *en* can afford without a great loss of energy. However, the *en* ligand can take a meridional position in a *TBP* or in a *SP* structure (($a_2$) and ($a_3$)) where the expected bite angle is ~90°. Locating *en* in the base of a *SP* and moving Pt above the base plane would favour NPtN angles close to a least strained *en* structure with an angle of 80°.

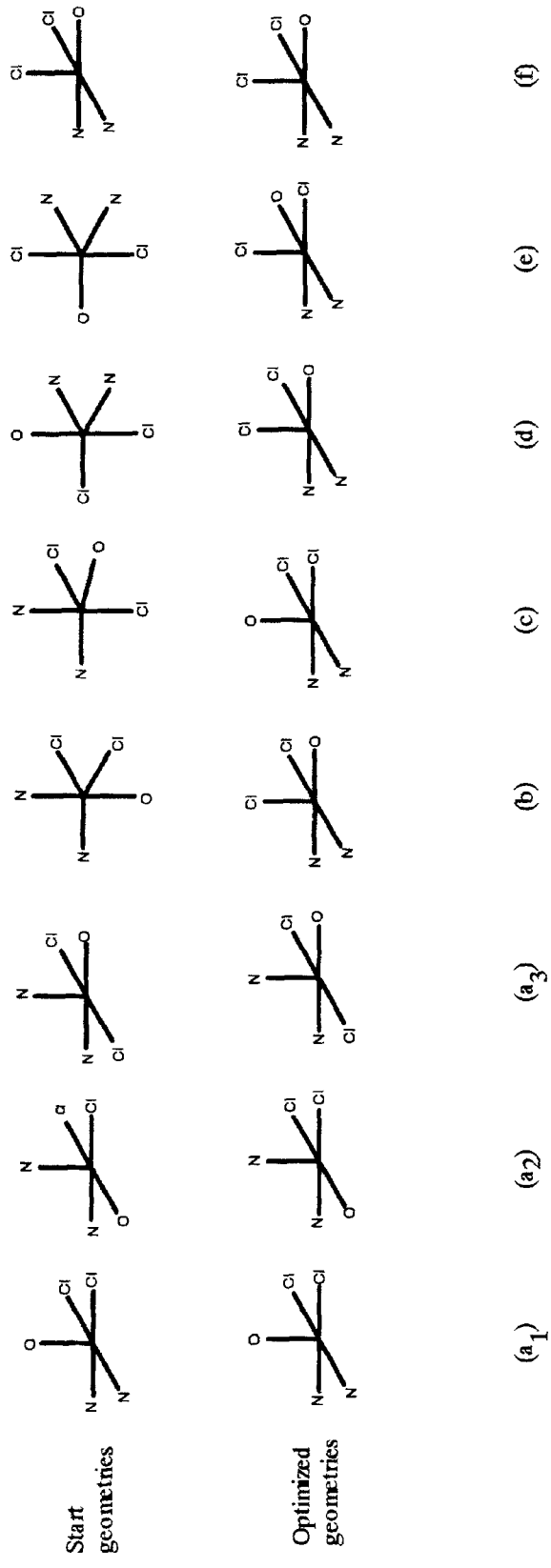


**Fig. 3.** Start and optimized geometries for Pt(*en*)$Cl_2$ ($H_2O$) transition state complexes; the notations are the same as in Fig. 2

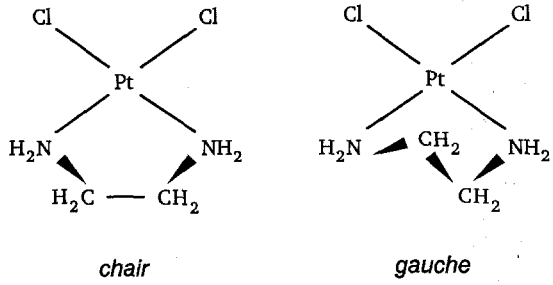


**Fig. 4.** *Chair* (left) and *gauche* (right) conformers of the *en* ligand in Pt(*en*)$Cl_2$ (**1**-$PtCl_2$)

The resulting structures with N at the apical position have higher *MM* energies (7.8 kcal · $mol^{-1}$, cases ($a_2$) and ($a_3$) in Table 1) than those with O or Cl at the apical position. The last structures (($a_1$) = (c)) have the same *MM* energy ($\sim$ 7.3 kcal · $mol^{-1}$) as (d) = (e), but different *EH* energies (−102.02, −101.74 eV, respectively). Structures (e) = (d) approach the *TBP* (one angle is close to 120° and another is close to 180°).

It should be thus concluded that the *SP* with Cl at the apex is the most favoured *TSC* structure from an entropy point of view.

In terms of *MM*, the order Cl $\approx$ O < N is obtained:

| Apical | Cl | O | N | |
|---|---|---|---|---|
| *MM* | 7.3–7.5 | 7.3 | 7.8 | kcal · $mol^{-1}$ |
| *EH* | −101.7 | −102.0 | −101.4 | eV |

In terms of *EH*, the most stable isomer is an *SP* with $H_2O$ at the apex. In fact, this is the *TSC* structure which retains most of the features of the reactant. Hence, both *MM* and *EH* indicate a planar [Pt(*en*)$Cl_2$] moiety with $H_2O$ at the apex. Both the *MM* and *EH* energies are very close, and once again the need of a better descriptor is evident.

For *en* and substituted *en* Pt compounds, both the stable symmetric (*gauche*, also called *envelope* structure) and the unstable asymmetric (*chair*, also called *half-chair* structure) conformers of the *en* ligand are considered (Fig. 4).

The *chair* conformations were always higher in *MM* energy than the *gauche* conformers; hence, the gauche conformers offer a lower energy path to the hydrolysis product. However, it should be noted that the *chair* conformers offer a slightly bigger $L \rightarrow M$ electron density shift as compared to the *gauche* conformer: $q$(Pt) (*chair*) < $q$(Pt) (*gauche*). Such a shift would facilitate the release of a negative chloride ion because of reduced electrostatic attraction with $Cl^-$. This finding indicates that a *gauche* → *chair* conformational change might facilitate the *TSC* decomposition to the reaction products. Only results for the stable symmetric *gauche* conformers are discussed further.

### *Pt(PhenPh)$Cl_2$($H_2O$)* (**2**-$PtCl_2(H_2O)$)

Three cases of a coordinated substituted *en* ligand stereoisomers were considered: *S,S* (> *d,l*), *R, R* (| *d,l*), and *R,S* (*meso*) (see Fig. 5). In Table 1, data only for the *S,S*

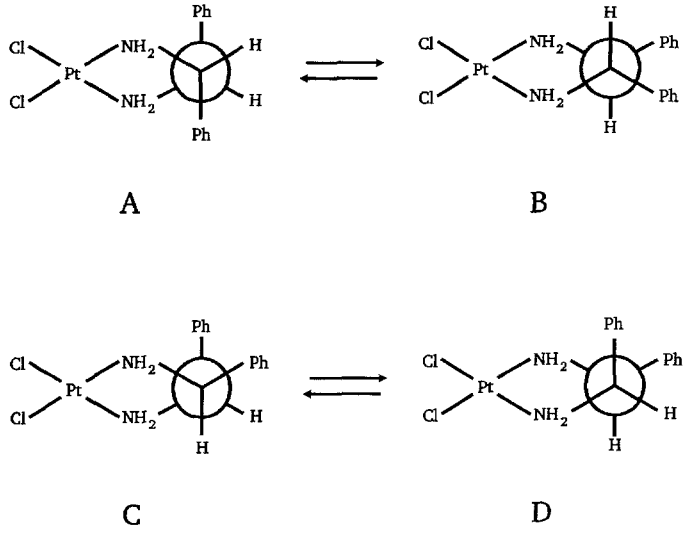


**Fig. 5.** Possible conformers of **2**-, **3**-, **4**-, and **5**-$PtCl_2$: *A*, *(R,R)*; *B*, *(S,S)*; C and *D*, *(R,S)*

forms are shown; the data for the other two *(R,R* and *R,S),* are compared in Table 2 (for **2**-$PtCl_2(H_2O)$) and in Table 3 (for **3**-$PtCl_2(H_2O)$). The diastereoisomers of **2**-$PtCl_2(H_2O)$ will be discussed together with those of **3**-$PtCl_2(H_2O)$ in the next section.

As expected, based on the results for the unsubstituted *en* complexes, the preferred *TSC* geometry is again an *SP* intermediate (Fig. 6). With the possible exception of structure ($a_2$), all other structures show two similar *trans*-basal angles (Table 1). Structures ($a_4$), (b), and (c) are equivalent (Fig. 6) and have the lowest *MM* energy, with (d) = (e) coming next with $\sim 0.2\,\text{kcal} \cdot \text{mol}^{-1}$ higher. These structures have also the lowest Pt charges. The numbers of occurrence are: 5 with Cl at the apex, 2 with N at the apex, and 1 with $H_2O$ at the apex. These indicate that an additional strucure with apical Cl is obtained. The new *SP* strucutre is produced from the *trans* $NH_3$-Cl *TBP* which gave an *SP* with $H_2O$ at the apex for the unsubstituted *en* complex. The reason for this change is unclear. A possible explanation is that the two *SP* structures with $H_2O$ at the apex ($a_1$) and *SP* with Cl at the apex (c) may have very close energies. As can be seen from Table 1 and Fig. 6, the difference is only $0.5\,\text{kcal} \cdot \text{mol}^{-1}$ *MM* energy.

| Apical | Cl | N | O | |
|---|---|---|---|---|
| *MM* | 24.3–24.5 | 25.9–26.9 | 24.8 | $\text{kcal} \cdot \text{mol}^{-1}$ |
| *EH* | −269.8 | −269.6 | −270.2 | eV |

The order in *MM* energy is Cl ≈ O < N and in *EH* energy O < Cl ≈ N, *i.e.* N is least probable and O and Cl are more probable with almost equal chances to get at the apex. In terms of entropy changes, however, the *SP* with O at the apex is less probable for **2**-$PtCl_2(H_2O)$ (occurs once) than for **1**-$PtCl_2(H_2O)$ (occurs twice). With almost equal *MM* and *EH* energies for apical Cl and $H_2O$ structures, the entropy factor may dominate to make the structure with Cl at the apex the most

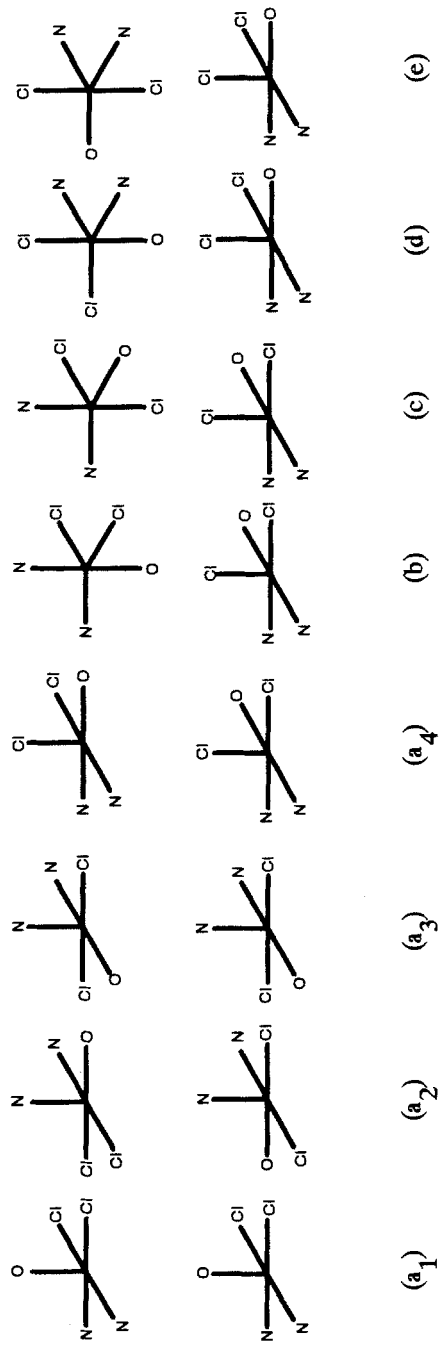


**Fig. 6.** Start and optimized geometries for the Pt(Ph*en*Ph)$Cl_2(H_2O)$ (**2**-$PtCl_2(H_2O)$) transition state complexes (notations as in Fig. 2)

favoured one. Such a structure would be best suited to decompose to the product by splitting the apical Cl–Pt bond.

*Pt(PhOHenPhOH)Cl$_2$(H$_2$O)* (**3**-PtCl$_2$(H$_2$O))

The results referring to the *S,S* conformer are given in Table 1 and Fig. 7.

The other conformers are discussed in section *A.2*. All *MM*-optimized structures are termed as *SP*, although in some cases ((b) = (c) = (d) and ($a_2$)) the two *trans*-basal angles are quite different, indicating that the geometry is far from a regular *SP*. It is distorted along the path to a *TBP* (see *Section B*) and structures ((b) = (c) = (d)) may be better termed as distorted *TBP* rather than distorted *SP*. For this reason, these structures are depicted as *TBP*s in Fig. 7. In this respect, the *MM*-optimized structures of **3**-PtCl$_2$(H$_2$O) span a picture different from that for **1**- and **2**-PtCl$_2$(H$_2$O): whereas the last two compounds prefer the *SP* with Cl at the apex, **3**-PtCl$_2$(H$_2$O) exhibits *SP* structures highly distorted along the path of conversion towards a *TBP* with $NH_3$ and Cl at the axial positions. The optimized structures take the order

| | *TBP* (N-Cl) or *SP* (N) | *SP* (O) | *SP* (Cl) | *SP* (N) | |
|---|---|---|---|---|---|
| *MM* | 23.0 | 22.6 | 23.1 | 23.2–24.0 | kcal·mol$^{-1}$ |
| *EH* | −279.4 | −279.5 | −279.5 | −279.4 | eV |
| | 3 | 1 | 2 | 2 | number of occurrence |

or

*SP* (O) < *TBP* (N-Cl) ≤ *SP* (Cl) < *SP* (N) in *MM*
*SP* (O) ≈ *SP* (Cl) < *TBP* (N-Cl) ≈ *SP* (N) in *EH*

It can be seen from the data given above that the energy differences are very small and the energy values are once again poor discriminators for the studied strucutres (see *Section B*). In view of the close energy values, the predominant factor may be the entropy related to the number of occurrences. This factor favours the least distorted (related to *SP*) structures (b) = (c) = (d), which in fact should be combined with ($a_2$) and ($a_3$), giving 5 *SP* structures with N at the apex.

The reason why a distorted *TBP* with N and Cl at apical positions is preferred over the other combinations (N-N, N-OH$_2$, Cl-Cl, Cl-O) is clear: as pointed out for *cis*-Pt($NH_3$)$_2$Cl$_2$(H$_2$O), one $NH_3$ always occupies an axial position in a *TBP*. From the options N-Cl, N-OH$_2$, and N-N, the last one is preferred as a *TSC* of cisplatin, but it is impossible for **1**-, **2**- and **3**-PtCl$_2$(H$_2$O) *TSC*s since it spans a NPtN angle of *en* amounting to 180°. The choice between N-OH$_2$ and N-Cl would depend – among other factors – upon the repulsion of the axial and equatorial ligands in a *TBP*. The N-Cl combination places H$_2$O in the equatorial plane where repulsion is less than in an axial position. It should be noted that the isomer with N and Cl in axial positions would offer the best arrangement for the *trans*-influence of N to be exerted upon the leaving $Cl^-$ ion. Such an effect is impossible if N and Cl were located in the equatorial plane of a *TBP*.

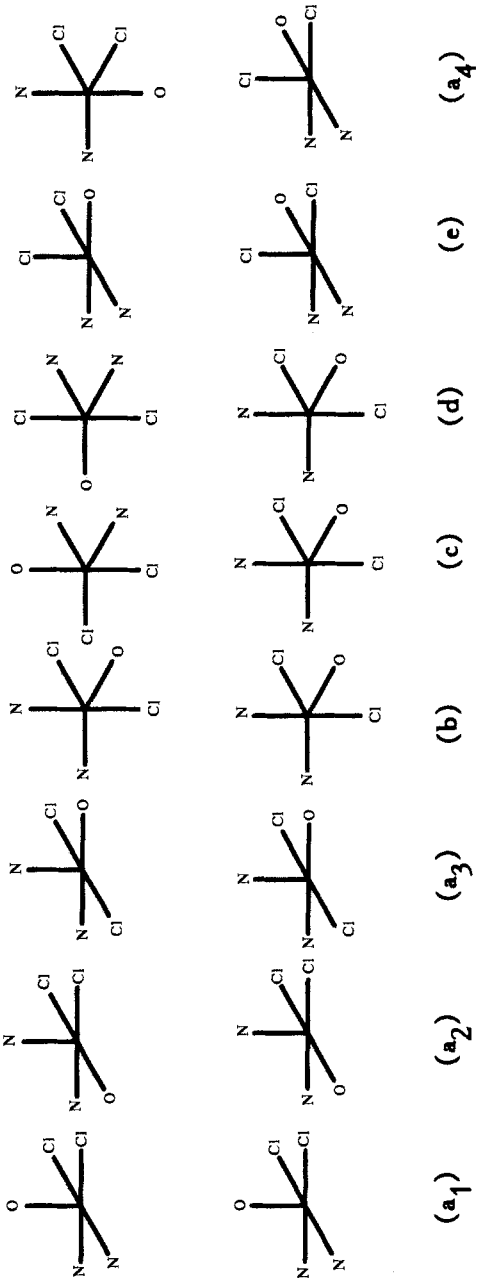


**Fig. 7.** Start and optimized geometries for Pt(PhOH*en*PhOH)$Cl_2(H_2O)$ (3-$PtCl_2(H_2O)$) transition state complexes (notations as in Fig. 2)

## 2. Diastereomers of **2**-$PtCl_2(H_2O)$ and **3**-$PtCl_2(H_2O)$

The results for the two diastereomers ((*R,R/S,S*) and (*R,S*), Fig. 5) for **2**-$PtCl_2(H_2O)$ are given in Table 2. In order to avoid local force-field minima, minimizations from several distinct input structures were carried out. Four structures, obtained as a result after *MM*-minimization for **1**-$PtCl_2(H_2O)$ ((a), (b), (c), (d), (e) and (f) – compound **2** in Table 1) have been selected as input, and the Ph groups have been added prior to the geometry optimization. The calculated structural data show that the (*R,R/S,S*) and (*R, S*) forms of the **2**-$PtCl_2(H_2O)$ *TSC*s are stabilized predominantly in *SP* (Cl or O at the apex) structures with almost equal *MM* energies (Table 2) or in a *SP* (N at the apex) structure with slightly higher *MM* energy. The *SP* forms, which show distortions towards a *TBP* structure, are the (*R,R*) and (*R,S*) forms of structure ($a_2$) (see *trans*-basal angles in Table 2). For all other structures studied here, both the (*R,R/S,S*) and the (*R,S*) forms were found to be stabilized as an *SP TSC*. The (*R,S*) form shows a slightly higher *MM* energy than the (*R,R/S,S*) forms ($\sim$0.5–1.0 kcal·mol$^{-1}$) with the exception of structure ($a_3$) where a difference of $\sim$2–5 kcal·mol$^{-1}$ was found.

**Table 2.** *MM*[a] and *SE*[a] energy data for the transition state complexes of the **2**-$PtCl_2(H_2O)$ conformers

| 2-$PtCl_2$ ($H_2O$) | | (*S,S*)[b] | (*R,S*)[b] | (*R,R*)[b] |
|---|---|---|---|---|
| *MM* Energy (kcal·mol$^{-1}$) | | | | |
| from structure ($a_1$) | | | | |
| *SP*, O-apical[c] | *MM* | 24.8 | 25.1 | 24.1 |
| | *SE* | 26.2 | 26.5 | 25.5 |
| *trans*-basal angles (°) | | 161 | 169 | 165 |
| | | 163 | 159 | 146 |
| from structure ($a_4$) = (b) = (c) | | | | |
| *SP*, Cl-apical | *MM* | 24.3 | 24.8 | 24.6 |
| | *SE* | 25.7 | 26.2 | 25.9 |
| *trans*-basal angles (°) | | 159 | 158 | 163 |
| | | 155 | 164 | 145 |
| from structure (d) = (e) | | | | |
| *SP*, Cl apical | *MM* | 24.5 | 25.1 | 23.9 |
| | *SE* | 25.8 | 26.5 | 25.2 |
| *trans*-basal angles (°) | | 159 | 170 | 166 |
| | | 156 | 154 | 142 |
| from structure ($a_2$) | | | | |
| *SP*, N apical[c] | *MM* | 25.9 | 27.5 | 25.3 |
| | *SE* | 27.2 | 28.8 | 26.6 |
| *trans*-basal angles (°) | | 172 | 174 | 169 |
| | | 158 | 137 | 126 |
| from structure ($a_3$) | | | | |
| *SP*, N-apical | *MM* | 26.9 | 31.9 | 30.7 |
| | *SE* | 28.2 | 33.2 | 32.0 |
| *trans*-basal angles (°) | | 174 | 157 | 169 |
| | | 171 | 150 | 157 |

[a] *MM:* Molecular Mechanics energies, *SE*: Strain Energies; [b] *gauche* forms; [c] *SP*→ *TBP*

The study of the (*R,R/S,S*) and (*R, S*) forms of **3**-$PtCl_2(H_2O)$ provides additional information on the preferred *TSC* conformations. The same four conformations as for **2**-$PtCl_2(H_2O)$ have been investigated, but the results from the *MM*-optimization, with respect to the differences between (*R,R/S,S*) and (*R,S*), are quite different (Table 3). The (*R,S*) forms again show a higher energy as compared to both (*R, R/S,S*) forms, but the energy difference is about ~2–8 kcal·mol$^{-1}$, and the (*S,S*) conformer has the lowest energy.

Different positions of OH groups (in 3- and 4-positions in the benzene ring) for the hydroxyphenyl group have also been investigated (Table 3). The results for 3-

**Table 3.** *MM*[a] and *SE*[a] energy data for **2**-, **3**-, **4**-, and **5**-$PtCl_2(H_2O)$ *TSC*s with *SP* geometry

| *MM* Energy (kcal·mol$^{-1}$) | | *(S,S)*[b] | *(R,S)*[b] | *(R,R)*[b] |
|---|---|---|---|---|
| **3**-$PtCl_2(H_2O)$ | | | | |
| from structure ($a_1$) | | | | |
| *SP*, O apical | *MM* | 22.6 | 25.1 | 24.7 |
| | *SE* | 24.0 | 26.4 | 26.0 |
| *trans*-basal angles (°) | | 168 | 168 | 162 |
| | | 155 | 135 | 162 |
| from structure ($a_4$) = (e) | | | | |
| *SP*, Cl apical | *MM* | 23.0 | 25.5 | 24.2 |
| | *SE* | 24.4 | 26.8 | 25.5 |
| *trans*-basal angles (°) | | 160 | 171 | 168 |
| | | 154 | 159 | 149 |
| from structure (b) = (c) = (d) | | | | |
| *SP*, Cl apical | *MM* | 23.0 | 25.2 | 23.9 |
| | *SE* | 24.3 | 26.5 | 25.3 |
| *trans*-basal angles (°) | | 172 | 170 | 169 |
| | | 142 | 159 | 149 |
| from structure ($a_2$) | | | | |
| *SP*, N apical | *MM* | 23.2 | 28.2 | 25.4 |
| | *SE* | 24.5 | 29.6 | 26.7 |
| *trans*-basal angles (°) | | 173 | 180 | 171 |
| | | 157 | 144 | 142 |
| from structure ($a_3$) | | | | |
| *SP*, N apical | *MM* | 24.0 | 32.2 | 30.3 |
| | *SE* | 25.3 | 33.5 | 31.6 |
| *trans*-basal angles (°) | | 172 | 158 | 154 |
| | | 168 | 150 | 154 |
| **4**-$PtCl_2(H_2O)$ from structure (b) | *MM* | 23.2 | 23.5 | 23.6 |
| | *SE* | 24.6 | 24.8 | 24.9 |
| **5**-$PtCl_2(H_2O)$ from structure (b) | *MM* | 23.1 | 23.3 | 23.0 |
| | *SE* | 24.4 | 24.7 | 24.4 |
| **2**-$PtCl_2(H_2O)$ from structure (b) | *MM* | 24.3 | 24.8 | 24.6 |
| | *SE* | 25.7 | 26.2 | 25.9 |

[a] *MM*: Molecular Mechanical energies, *SE:* Strain Energies; [b] *gauche* forms

and 4-hydroxyphenyl substituted *TSC*s (**4**-$PtCl_2(H_2O)$ and **5**-$PtCl_2(H_2O)$) are very similar to those for the unsubstituted phenyl *TSC*s (**2**-$PtCl_2(H_2O)$): the (*R,R/S,S*) forms have approximately the same *MM* energy and the (*R,S*) and (*R,R/S,S*) forms differ only slightly.

The 2-hydroxyphenyl *TSC* (**3**-$PtCl_2(H_2O)$) has the lowest *MM* energy in the (*S,S*) conformation for all studied structures. The (*R,R*) form as well as the (*R,S*) form are stabilized as intermediates between *SP* and *TBP* with higher *MM* energy. Both results – the lower *MM* and electronic energies for the (*S,S*) form and the significant *MM* energy difference between (*R,R/S,S*) and (*R,S*) forms – could explain the faster hydrolysis reaction of the (*S,S*) form as compared with that of the (*R,S*) form of the **3**-$PtCl_2$ complex [28].

### *B. Description of Transition State Complex Geometries in Terms of a Distortion Vector*

The calculated geometries whose energies and structural data are listed in Tables 1, 2, and 3 have been referred to as trigonal *TBP* or *SP* on the basis of the calculated *trans*-axial (in *TBP*) and *trans*-basal (in *SP*) angles. The values of these angles help to determine the limiting cases (*TBP* or *SP*) but they do not reveal how much the real structures deviate from the ideal *TBP* or *SP*. At the same time, the *TBP* geometries obtained for $Pt(NH_3)_2Cl_2(H_2O)$ have equal or very similar *MM* and *EH* energies and thus they cannot be reliably discerned. The calculated *SP* geometries for the $Pt(NH_3)_2Cl_2(H_2O)$ analogues are also very close in energy. In order to discriminate the calculated geometries as well as to determine the degree of distortion away from the ideal *TBP* or *SP*, the structures are further discussed in terms of a total displacement (distortion) vector *D* as defined in Ref. [25].

We are mainly interested in distinguishing whether a given geometry is closer to an ideal *TBP* or to an ideal *SP*, *i.e.* to position the structure on the *SP-TBP* conversion path. We have calculated the distortion away from the idealized structures in the 12-dimensional space defined by the complete set of displacement coordinates (Tables 4, 5, 6; Figs. 8, 9).

**Table 4.** Displacement coordinates for *TBP* ($D_{3h}$) [25][a]

| | |
|---|---|
| $A_1'$ | $S_1 = 2^{-1/2}(\Delta r_1 + \Delta r_5)$ |
| | $S_2 = 3^{-1/2}(\Delta r_2 + \Delta r_3 + \Delta r_4)$ |
| $A_2''$ | $S_3 = 2^{-1/2}(\Delta r_1 - \Delta r_5)$ |
| | $S_4 = 6^{-1/2}(\Delta\theta_{12} + \Delta\theta_{13} + \Delta\theta_{14} - \Delta\theta_{25} - \Delta\theta_{35} - \Delta\theta_{45})$ |
| $E'$ | $S_{5a} = 6^{-1/2}(2\Delta r_3 - \Delta r_2 - \Delta r_4)$ |
| | $S_{5b} = 2^{-1/2}(\Delta r_2 - \Delta r_4)$ |
| | $S_{6a} = 6^{-1/2}(2\Delta\theta_{24} - \Delta\theta_{34} - \Delta\theta_{23})$ |
| | $S_{6b} = 2^{-1/2}(\Delta\theta_{34} - \Delta\theta_{23})$ |
| | $S_{7a} = 12^{-1/2}(\Delta\theta_{13} - \Delta\theta_{12} - \Delta\theta_{14} + 2\Delta\theta_{35} - \Delta\theta_{25} - \Delta\theta_{45})$ |
| | $S_{7b} = 1/2(\Delta\theta_{12} - \Delta\theta_{14} + \Delta\theta_{25} - \Delta\theta_{45})$ |
| $E''$ | $S_{8a} = 12^{-1/2}(2\Delta\theta_{13} - \Delta\theta_{12} - \Delta\theta_{14} - 2\Delta\theta_{35} + \Delta\theta_{25} + \Delta\theta_{45})$ |
| | $S_{8b} = 1/2(\Delta\theta_{12} - \Delta\theta_{14} - \Delta\theta_{25} + \Delta\theta_{45})$ |

[a] $\Delta r_i$ are deviations of the calculated bond lengths from the standard ones, $\Delta\theta_{ij}$ are differences between the angles of the idealized and the *MM* optimized molecules

**Table 5.** Displacement coordinates for *SP* ($C_{4v}$)[25][a]

| | |
|---|---|
| $A_1$ | $S_1 = \Delta r_3$ |
| | $S_2 = 1/2(\Delta r_1 + \Delta r_2 + \Delta r_4 + \Delta r_5)$ |
| | $S_3 = 2^{-1/2}(\Delta\theta_{15} + \Delta\theta_{24})$ |
| $B_1$ | $S_4 = 1/2(\Delta r_1 + \Delta r_5 - \Delta r_2 - \Delta r_4)$ |
| | $S_5 = 2^{-1/2}(\Delta\theta_{15} - \Delta\theta_{24})$ |
| $B_2$ | $S_6 = 1/2(\Delta\theta_{12} + \Delta\theta_{45} - \Delta\theta_{14} - \Delta\theta_{25})$ |
| $E$ | $S_{7a} = 2^{-1/2}(\Delta r_1 - \Delta r_5)$ |
| | $S_{7b} = 2^{-1/2}(\Delta r_4 - \Delta r_2)$ |
| | $S_{8a} = 2^{-1/2}(\Delta\theta_{13} - \Delta\theta_{35})$ |
| | $S_{8b} = 2^{-1/2}(\Delta\theta_{34} - \Delta\theta_{23})$ |
| | $S_{9a} = 2^{-1/2}(\Delta\theta_{12} - \Delta\theta_{45})$ |
| | $S_{9b} = 2^{-1/2}(\Delta\theta_{14} - \Delta\theta_{25})$ |

[a] $\Delta r_i$ are deviations of the calculated bond lengths from the standard ones, $\Delta\theta_{ij}$ are differences between the angles of the idealized and the *MM* optimized molecules

**Table 6.** Reference angles ($\theta_{ij}$, °) for *TBP* and *SP*[a]

| Angle | *TBP* | *SP* |
|---|---|---|
| $\theta_{12}$ | 90 | 86 |
| $\theta_{13}$ | 90 | 105 |
| $\theta_{14}$ | 90 | 86 |
| $\theta_{23}$ | 120 | 105 |
| $\theta_{24}$ | 120 | 150 |
| $\theta_{34}$ | 120 | 105 |
| $\theta_{25}$ | 90 | 86 |
| $\theta_{35}$ | 90 | 105 |
| $\theta_{45}$ | 90 | 86 |
| $\theta_{15}$ | 180 | 150 |

[a] The numbering is according to Fig. 8

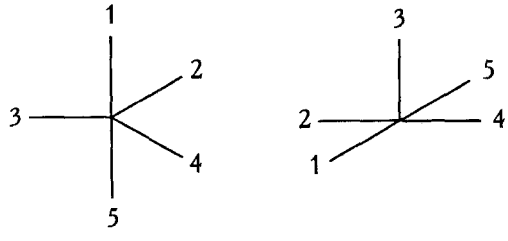


*TBP* *SP*

**Fig. 8.** Ligand numbering for trigonal bipyramid and square pyramid

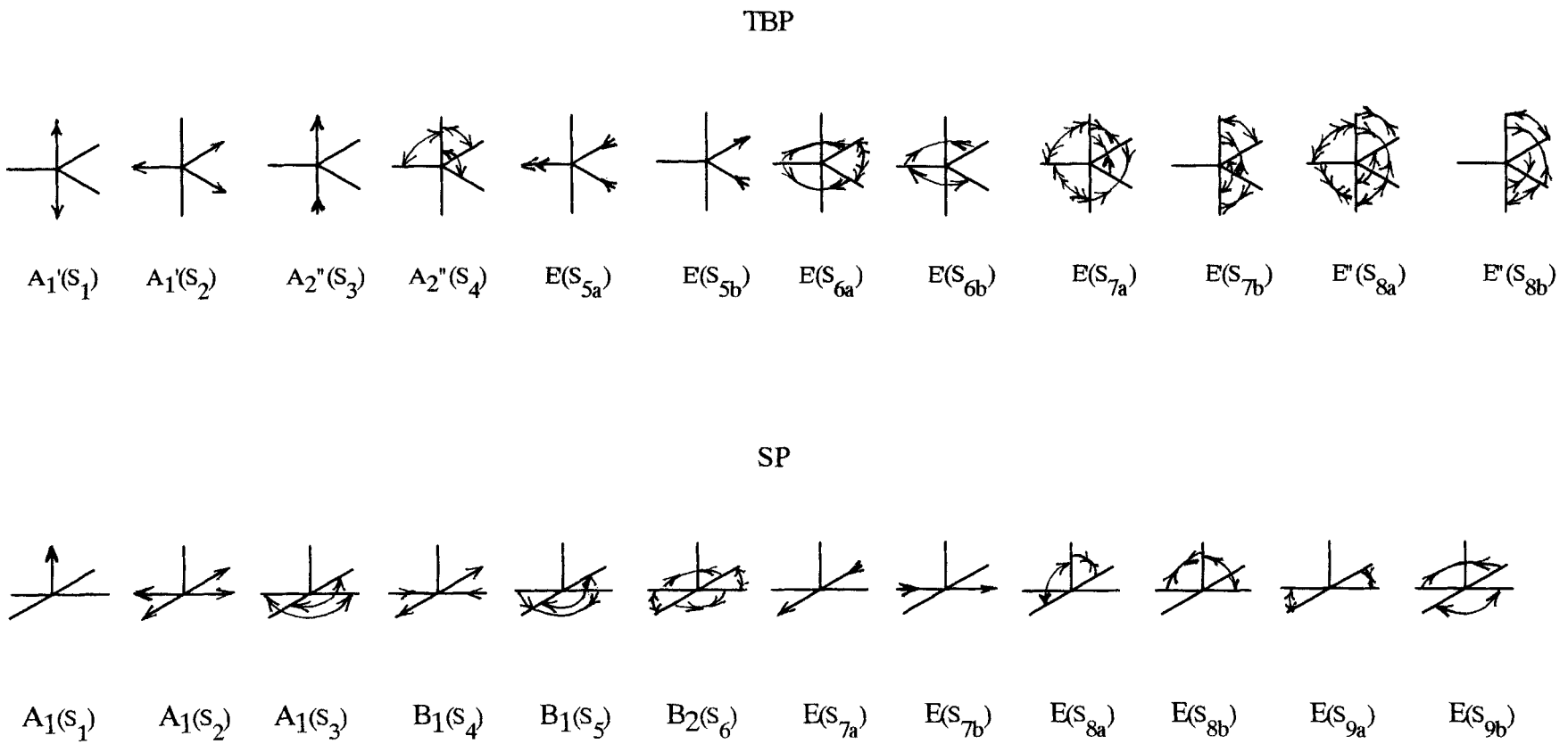


**Fig. 9.** Graphic illustration of the displacement coordinates (symmetry modes) for $D_{3h}$ (trigonal bipyramid, first row) and $C_{4v}$ (square pyramid, second row)

The contributions of the displacement coordinates involving bond stretching to the distortion vector are in general small; however, they are of special interest since they combine among themselves (*i.e.* $A_1' \rightarrow (S_1 - S_2)$ for *TBP*, $A_1 \rightarrow (S_1+S_2)$, $(S_1+S_3), (-S_2+S_3)$ for *SP*) and they also combine with the displacement coordinates that involve bending (*i.e.*) $E' \rightarrow (S_{5a}+S_{6a})$, $A_2'' \rightarrow (S_3 - S_4)$, (see Fig. 9). The *Berry* twist [25, 29] is $(S_{6a}+S_{7a})$, and the umbrella type coordinate [25] is $(S_3 - S_4)$ (*vide infra*). The combinations $(S_1 - S_2)$ in *TBP* space and $(S_1+S_2)$, $(S_1+S_3)$, and $(-S_2+S_3)$ in *SP* space are related to the constant-amount-of-glue distortion [25].

The calculated values of the distortion vector are given in Tables 7, 8, 9, and 11. The leading symmetry coordinates for *TBP* and *SP* deformations, according to Fig. 9, are also given there.

We shall again discuss the four compounds, this time with respect to their *DV* values and displacement coordinate contributions.

### *$Pt(NH_3)Cl_2(H_2O)$*

Table 7 lists the calculated *DV*s and the active displacement coordinates. It can be seen from Fig. 2 and Table 7 that the *TBP* structures have *DV* values which are smaller for *TBP* than for *SP*; *vice versa,* the structure classified as *SP* has a smaller *DV* value for *SP* than for *TBP*. Hence, the classification to *TBP* or *SP* made previously on inspection of the *MM* data (energies and angles) is also quantitatively correct. However, the *DV* values offer a chance to better discriminate the *MM* geometries obtained with equal or almost equal *MM* energies. A survey of the *DV* values shows that the least distorted geometry is $a_2$ (Fig. 2; *DV* in *TBP* space = 0.27), a *TBP* with N-N *trans*-axial donor atoms. The leading displacement coordinates for all *TBPs* are of $E'$ symmetry, the most active components being $S_6 > S_7 > S_5$. The combination $(S_{6a}+S_{7a})$ reflects the *Berry* twist with one equatorial ligand (atom 3, see Fig. 8) acting as pivot [25]. Mixing the stretching $S_{5a}$ to the *Berry* coordinates increases the pivot bond length, whereas the other two equatorial ligands move towards the metal and away from each other by increasing the angle $\theta_{24}$ (see again Fig. 8 and Ref. [10c]).

Table 7 demonstrates that there is also a net contribution of the totally symmetric coordinate $A_1'$ and of $A_2''$ to produce the distorted *TBP* structure. This multi-mode action has been discussed in detail elsewhere [25, 10c]. It indicates that a *vibronic* mechanism may be responsible for shaping the 5-coordinate *TSC*.

The *TBP* geometries with N-Cl *trans*-axial atoms show higher *DV* values as compared with the *TBP* structures with N-N *trans*-axial atoms; hence, they are more distorted *TBP*s. In addition, the $E''$ coordinate contributes to the distortion (components $S_{8b}$ and $S_{8a}$), further reducing the symmetry. The three *TBP* geometries with N-O *trans*-axial atoms show even higher *DV* values. Instead of the $E''$ coordinate, the second active one is that of $A_2''$ symmetry. The combination of the two components of $A_2''$ $(S_3 - S_4)$ represents the umbrella type distortion, which is operational only for the *trans* N-O axial geometries.

Our results suggest that the deformations of a given *TSC* structure away from a *TBP* towards *SP* (or *vice versa*) are to a large extent independent of bond length distortions; however, some stretching modes (*vide supra*), although with modest

**Table 7.** *MM* energy and distortion vector values for different geometries of $Pt(NH_3)_2Cl_2(H_2O)$ in *TBP* and SP spaces[a]

| Geometry | ($a_1$) | ($a_2$) | ($a_3$) | ($a_4$) | (b) | (c) | (d) | (e) | (f) |
|---|---|---|---|---|---|---|---|---|---|
| *MM* energy (kcal·mol$^{-1}$) | 8.1 | 7.5 | 8.0 | 8.0 | 8.0 | 8.0 | 7.7 | 7.7 | 8.0 |
| *DV* (*TBP* space) | 1.56 | 0.27 | 1.37 | 1.37 | 1.52 | 1.40 | 0.33 | 0.29 | 0.49 |
| *DV* (*SP* space) | 0.66 | 1.85 | 2.75 | 2.76 | 2.99 | 2.98 | 2.34 | 1.83 | 1.96 |
| Active modes | *E* | *E'* | *E'* | *E'* | *E'* | *E'* | *E'* | *E'* | *E'* |
| (Predominant | (7a, 7b, 8a, 8b, 9a) | (6a, 7a, 5a) | (6a, 6b, 7b, 5a) | (6a, 6b, 7b, 5a) | (6a, 6b, 7b, 5a) | (6a, 6b, 5a, 5b) | (6a, 6b, 5a) | (6a, 7b, 5a) | (6a, 6b, 5a, 5b) |
| symmetry | – | – | $A_2''$ | $A_2''$ | $A_2''$ | $E''$ | – | – | $E''$ |
| coordinates) | – | – | (4, 3) | (4, 3) | (4, 3) | (8b, 8a) | – | – | (8a, 8b) |
| | $A_1$ | $A_1'$ | $A_1'$ | $A_1'$ | $A_1'$ | $A_1'$ | $A_1'$ | $A_1'$ | $A_1$ |
| | (1, 2, 3) | (1, 2) | (1, 2) | (1, 2) | (1, 2) | (1, 2) | (1, 2) | (1, 2) | (1, 2) |

[a] The letters (a)–(f) have the same meaning as in Fig. 2

contributions to the *DV* values, are essential in shaping the ultimate *TSC* geometry.

### *Pt(en)Cl$_2$(H$_2$O)* (**1**-PtCl$_2$(H$_2$O))

From the geometric parameters calculated for Pt(*en*)Cl$_2$(H$_2$O) (Table 1), it is evident that all structures, with the possible exceptions of ($a_2$), (d), and (e), have two angles that are close to each other and higher than 150°. These structures should be termed as square based pyramids with different Pt elevation above the basal plane. A survey of the calculated *DV* values (Table 8) shows that all structures have *DV(SP)* < *DV(TBP)* which is consistent with the drawings adopted in the second row in Fig. 3. Hence, the *DV* values, as in the case of [Pt(NH$_3$)$_2$Cl$_2$(H$_2$O)], are a much more sensitive descriptor of the *TSC* structures than the absolute values of the valence angles or the *MM* energies.

The leading displacement coordinate for all output geometries of [Pt(*en*)Cl$_2$-(H$_2$O)] is that of *E*-symmetry in the *SP* space. The components that play a major role in shaping the geometry are $S_{7a}, S_{7b}, S_{8a}, S_{8b}, S_{9a}$, and $S_{9b}$ (according to Fig. 9). A slight distortion along the *Berry* twist path from *SP* space towards *TBP* is also observed ($B_1$-symmetry, components $S_4$ and $S_5$). The combination of $S_1$ and $S_2$ distortions reflects the constant-amount-of-glue displacement [25] that is equivalent to the $S_1$ and $S_2$ combination of a *TBP* being distorted towards a *SP*. This distortion is typical for [Pt(*en*)Cl$_2$(H$_2$O)]. In addition, there are two other combinations which are also important for the *SP* space: $(S_1 + S_3)$ and $(S_3 - S_2)$. Together with $(S_1 + S_2)$ they are the most important modes for a classical reversible association reaction of a square planar centre [25].

The least distorted *TSC* structure is an *SP* with Cl at the apex ((f) = (b) = (d)). The small *MM* energy differences for the 4 *SP* structures with apical Cl are also not significant in terms of the *DV*(SP) values, structure (e) being a slightly more distorted *SP* than (f), (b), and (d).

### *Pt(PhenPh)Cl$_2$(H$_2$O)* (2-PtCl$_2$(H$_2$O))

The *MM*-optimized structures are treated as *SP* since the two *trans*-basal angles are equal, with the possible exception of ($a_2$) (Table 2, Fig. 6). However, a comparison between *DV*(SP) and *DV*(TBP) (Table 9) shows that all structures should be classified as *SP* and the only exception is ($a_3$), not ($a_2$). This is a demonstration of the better discriminating ability of *DV* as compared with the use of single *MM* data (energies or angles). Therefore, the ($a_3$) structure should be termed as *TBP*; in fact it is the least distorted *TBP*. The least distorted *SP* structures with apical Cl are (b) = (c) = (e) = ($a_4$) ≈ (d) (*DV* = 0.6–0.8, Table 9). Higher *DV*s are obtained for *SP* with apical OH$_2$ (*DV* = 0.91) and *SP* with apical N (*DV* = 1.4–1.8). Judging from the *trans*-basal values, the structures with apical N are nearly T-shaped ($C_{2v}$ symmetry), whereas those with apical OH$_2$ and especially with apical Cl typically exhibit a high elevation of Pt above the basal plane.

The leading *SP* symmetry coordinate for all *TSC*s of **2**-PtCl$_2$(H$_2$O) is of E symmetry, with main components $S_{7b}, S_{7a}, S_{8a}$, and $S_{8b}$ shown in Table 9. These

**Table 8.** *MM* energy and distortion vector values for different *MM*-optimized geometries of Pt(*en*)$Cl_2(H_2O)$ (**1**-$PtCl_2(H_2O)$) in *SP* and *TBP* spaces[a]

| Geometry | ($a_1$) | ($a_2$) | ($a_3$) | (b) | (c) | (d) | (e) | (f) |
|---|---|---|---|---|---|---|---|---|
| *MM* energy ($kcal \cdot mol^{-1}$) | 7.32 | 7.78 | 7.80 | 7.48 | 7.33 | 7.28 | 7.26 | 7.46 |
| *DV* (*SP* space) | 0.93 | 1.35 | 1.96 | 0.67 | 1.04 | 0.66 | 0.85 | 0.66 |
| *DV* (*TBP* space) | 1.77 | 1.81 | 2.66 | 1.85 | 1.51 | 1.64 | 1.34 | 1.85 |
| Active modes | *E* | *E* | *E* | *E* | *E* | *E* | *E* | *E* |
| (Predominant | (7b, 8a, 8b) | (7b, 8a, 8b) | (7a, 7b, 8a, 8b) | (7a, 7b, 8a) | (7a, 7b, 8a, 8b) | (7b, 8a, 8b) | (8a, 7b, 8b) | (7a, 7b, 8a) |
| symmetry | $B_1$ | $B_1$ | $B_1$ | – | $B_1$ | – | $B_1$ | – |
| coordinates) | (4) | (4, 5) | (4, 5) | – | (4) | – | (4) | – |
| | $A_1$ | $A_1$ | $A_1$ | $A_1$ | $A_1$ | $A_1$ | $A_1$ | $A_1$ |
| | (1, 2, 3) | (1, 2, 3) | (1, 2, 3) | (1, 2, 3) | (1, 2, 3) | (1, 2, 3) | (1, 2, 3) | (1, 2, 3) |

[a] The letters (a)–(f) have the same meaning as in Fig. 3

**Table 9.** *MM* energy and distortion vector values for different *MM*-optimized geometries of Pt(Ph*en*Ph)$Cl_2(H_2O)$(**2**-Pt$Cl_2(H_2O)$) in *SP* and *TBP* spaces[a]

| Geometry | ($a_1$) | ($a_2$) | ($a_3$) | ($a_4$) | (b) | (c) | (d) | (e) |
|---|---|---|---|---|---|---|---|---|
| *MM* energy (kcal·mol$^{-1}$) | 24.8 | 25.9 | 26.9 | 24.3 | 24.3 | 24.3 | 24.5 | 24.5 |
| *DV* (*SP* space) | 0.91 | 1.42 | 1.81 | 0.63 | 0.64 | 0.63 | 0.77 | 0.64 |
| *DV* (*TBP* space) | 2.01 | 1.88 | 1.50 | 1.83 | 1.79 | 1.82 | 1.89 | 1.83 |
| Active modes | *E* | *E* | *E'* | *E* | *E* | *E* | *E* | *E* |
| (Predominant | (7b, 8a, 7a, 8b) | (6b, 6a, 5b, 7a) | (7b, 7a, 8a, 8b) | (8a, 7b, 7a) | (8a, 7b, 7a) | (8a, 7b, 7a) | (8a, 7b, 7a) | (8a, 8b, 7b) |
| symmetry | – | $A_2''$ | $B_1$ | – | – | – | – | – |
| coordinates) | – | (4, 3) | (4, 5) | – | – | – | – | – |
| | $A_1$ | – | $A_1'$ | $A_1$ | $A_1$ | $A_1$ | $A_1$ | $A_1$ |
| | (1, 2, 3) | – | (1, 2) | (1, 2, 3) | (1, 2, 3) | (1, 2, 3) | (1, 2, 3) | (1, 2, 3) |

[a] The letters (a)–(e) have the same meaning as in Fig. 6

modes are mixed with the totally symmetric $A_1$ mode to provide, as for **1**-$PtCl_2(H_2O)$, the actual distortion as a multi-mode vibronic process.

Concerning the possible different conformers, the calculated *DV* values in Table 11 show that in single cases the *TBP* geometry should be selected *e.g.* ($a_3$) for the (*S,S*) conformer. However, it should be pointed out that *TBP* is the preferred geometry for the (*R,R*) conformers (with the exception of ($a_3$) and (c) geometries), although the *DV*(*TBP*)-*DV*(*SP*) differences are small. A possible explanation of this finding could be that the axially oriented phenyl substituents of (*R,R*) are directed towards the O or Cl atoms at apical positions, and *SP* has to be distorted towards *TBP* in order to avoid the increased repulsion above the *TBP* equatorial plane. The (*R,S*) isomers have only one axial phenyl substituent, which in all cases is directed below the base of the square pyramid where the repulsion is much smaller as compared to the crowded axial positions in *TBP TSC*s of **2**-$PtCl_2(H_2O)$. Therefore, all (*R, S*) isomers with no exception should be closer to *SP* than to *TBP*. The displacement coordinates that play a major role for the *SP* deformation are: $E(S_{7a}, S_{7b}, S_{8a}, S_{8b}) > B_1(S_4, S_5) > A_1(S_1, S_2)$ (ordered with decreasing contribution). The $B_1$-modes ensure that the *SP* distortion is towards a *TBP*, although the large contribution of *E* modes takes the structure out of the *SP* → *TBP* deformation path.

### *Pt(PhOHenPhOH)Cl₂(H₂O)* (**3**-$PtCl_2(H_2O)$)

A survey of the *DV* data for **3**-$PtCl_2(H_2O)$ in Tables 10 and 11 displays a very complicated picture.

a) The least-distorted structures ($DV = 0.66$) are ($a_4$) and (e) (*i.e.* the (*S,S*) conformers with Cl at the apical position). This is in contrast with *MM* results which point to *TBP* structures (b), (c), and (d) (*trans*-axial N-Cl) with minimum *MM* energy. In terms of *DV*, (b), (c), and (d) are two times more distorted than ($a_4$) and (e). It may be thus concluded that the difference in *MM* energy (23.0 kcal·mol$^{-1}$ for (b), (c), and (d) and 23.1 kcal·mol$^{-1}$ for ($a_4$) and (e)), on which the previous distinction was made, is not significant; it is in fact below the expected accuracy of the *MM* results.

b) The second row in Fig. 7 depicts the optimized structures for the (*S,S*) conformer. Table 10 shows that structures (b), (c), and (d) should be termed as *TBP* with small differences as compared to *SP* (*DV*(*TBP*)-*DV*(*SP*) = 0.04). This picture for the (*S,S*) conformer is not retained for the (*R,S*) and (*R,R*) conformers (Table 11). Structures (b), (c), and (d) with a (*R, S*) conformation are less distorted as *SP*s (*DV*(*SP*)=1.18) than as *TBP*s (*DV*(*TBP*)=1.71). The opposite holds for the (*R,R*) conformers which like the (*S,S*) conformers prefer the *TBP* shape (*DV*(*SP*) = 1.11, *DV*(*TBP*)=0.96). The differences are small and indicate that all conformers are almost midway between *SP* and *TBP*.

c) An *SP* structure with Cl at the apical position is expected to favour the split of $Cl^-$ if *SP* is elongated with Cl at the apex. In the *SP* base, the N atoms exert *trans*-influence with respect to the $H_2O$ molecule and make it leave the *TSC*, thus favouring the reverse (deaquation) reaction. Hence, two conflicting trends are operative for the elongated *SP* with Cl at the apex. In fact, our *MM* results for Pt-Cl bond lengths indicate that the basal Pt-Cl is always longer than the Pt-Cl axial bond

**Table 10.** *MM* energy and distortion vector values for different *MM*-optimized geometries of $Pt(PhOH\textit{en}PhOH)Cl_2(H_2O)$ (**3**-$PtCl_2(H_2O)$) in *SP* and *TBP* spaces[a]

| Geometry | ($a_1$) | ($a_2$) | ($a_3$) | ($a_4$) | (b) | (c) | (d) | (e) |
|---|---|---|---|---|---|---|---|---|
| *MM* energy ($kcal \cdot mol^{-1}$) | 22.6 | 23.2 | 24.0 | 23.1 | 23.0 | 23.0 | 23.0 | 23.1 |
| *DV* (*SP* space) | 1.05 | 1.34 | 1.53 | 0.66 | 1.22 | 1.22 | 1.22 | 0.66 |
| *DV* (*TBP* space) | 1.65 | 1.61 | 2.46 | 1.76 | 1.18 | 1.18 | 1.18 | 1.76 |
| Active modes | *E* | *E* | *E* | *E* | *E* | *E* | *E* | *E* |
| (Predominant | (7b, 8a, 9a) | (7b, 8a, 8b, 7a) | (7a, 7b, 8a, 8b) | (8a, 7b) | (6a, 6b, 5a) | (6a, 6b, 5a) | (6a, 6b, 5a) | (8a, 7b) |
| symmetry | $B_1$ | $B_1$ | $B_1$ | – | $A_2''$ | $A_2''$ | $A_2''$ | – |
| coordinates) | (4, 5) | (4, 5) | (4, 5) | – | (3, 4) | (3, 4) | (3, 4) | – |
| | $A_1$ | $A_1$ | $A_1$ | $A_1$ | $A_1'$ | $A_1'$ | $A_1''$ | $A_1$ |
| | (1, 2, 3) | (1, 2, 3) | (1, 2, 3) | (1, 2, 3) | (1, 2) | (1, 2) | (1, 2) | (1, 2, 3) |

[a] The letters (a)–(e) have the same meaning as in Fig. 7

**Table 11.** Distortion vectors in *SP* space ($DV_{SP}$) and in *TBP* space ($DV_{TBP}$) of (*S,S*), (*R,S*) and (*R,R*) isomers for different geometries of **2**-$PtCl_2$ ($H_2O$) (Pt(Ph*en*Ph)$Cl_2$($H_2O$)) and **3**-$PtCl_2$($H_2O$) (Pt(PhO-H*en*PhOH)$Cl_2$($H_2O$))

| Compound (structure) | (*S,S*) | | (*R,S*) | | (*R,R*) | |
|---|---|---|---|---|---|---|
| **2**-$PtCl_2$($H_2O$) | $DV_{SP}$ | $DV_{TBP}$ | $DV_{SP}$ | $DV_{TBP}$ | $DV_{SP}$ | $DV_{TBP}$ |
| ($a_1$) | 0.91 | 2.01 | 1.14 | 1.87 | 1.47 | 1.21 |
| ($a_2$) | 1.42 | 1.88 | 1.04 | 1.22 | 1.34 | 0.87 |
| ($a_3$) | 1.81 | 1.50 | 1.45 | 2.54 | 1.29 | 2.16 |
| ($a_4$) | 0.63 | 1.83 | 0.88 | 1.81 | 1.41 | 1.21 |
| (c) | 0.63 | 1.82 | 0.88 | 1.81 | 1.41 | 1.21 |
| (e) | 0.64 | 1.83 | 1.01 | 1.52 | 0.96 | 1.02 |
| (b) | 0.64 | 1.79 | 1.02 | 1.60 | 1.25 | 1.15 |
| (d) | 0.77 | 1.89 | 0.92 | 1.42 | 1.11 | 0.99 |
| **3**-$PtCl_2$($H_2O$) | | | | | | |
| ($a_1$) | 1.05 | 1.65 | 1.66 | 0.75 | 1.32 | 2.10 |
| ($a_2$) | 1.31 | 1.61 | 1.68 | 0.99 | 1.25 | 1.19 |
| ($a_3$) | 1.53 | 2.46 | 1.56 | 2.64 | 1.57 | 2.60 |
| ($a_4$) | 0.66 | 1.76 | 1.08 | 1.70 | 1.20 | 1.40 |
| (e) | 0.66 | 1.76 | 1.08 | 1.70 | 1.20 | 1.40 |
| (b) | 1.22 | 1.18 | 1.18 | 1.71 | 1.11 | 0.96 |
| (c) | 1.22 | 1.18 | 1.18 | 1.71 | 1.11 | 0.96 |
| (d) | 1.22 | 1.18 | 1.18 | 1.71 | 1.11 | 0.96 |

by 0.2–0.3 Å, and a compressed *SP* with Cl in the base and a strong in-base *trans*-effect should both contribute to make the basal $Cl^-$ leave the *TSC*.

The experimental kinetic data for the hydrolysis of (*S,S*) and (*R,S*) isomers of **3**-$PtCl_2$ correlate with our *DV* values: it is known that the (*S, S*) isomer hydrolysis is faster compared to the (*R, S*) isomer [28]. The data in Table 11 show that the (*S, S*) isomer of **3**-$PtCl_2$($H_2O$) is less distorted than the (*R, S*) isomer with *SP* shape. The least distorted *TSC* is expected to provide a lower energy barrier to the hydrolysis reaction than a *TSC* with a higher distortion, which is fully consistent with the available kinetic data.

By comparing the *DV* results it is seen that the *TSC*s of the **2**- and **3**-$PtCl_2$ ($H_2O$) compounds are more distorted as compared to those for cisplatin and **1**-$PtCl_2$($H_2O$). Obviously, additional deformations occur in **2**- and **3**-$PtCl_2$($H_2O$) due to the complicated ligand structure, and the discussed geometries are far away (possibly midway) from both ideal *TBP* and *SP*.

### *C. Energy Barriers*

Table 12 lists the changes in *MM* and *EH* energies when a Pt(II) complex reacts with a water molecule to form its *TSC*. The *MM* and *EH* values for the reactants are taken from Ref. [1], and the *MM* and *EH* of water have been added. The *TSC* energies are given in Table 1. It can be seen from Table 12 that the lowest barrier in terms of *MM* energy is offered by the (*S, S*) conformers of **2**- and **3**-$PtCl_2$($H_2O$)

**Table 12.** Differences between the *EH* and *MM* energies of the transition state complexes and reactants accompanying the hydrolysis reaction[a]

| Compound | *EH* | | | *MM* | | |
|---|---|---|---|---|---|---|
| | $\Delta EH$ (eV) | $\Delta q$(Cl) | $\Delta q$(Pt) | $\Delta MM$ (kcal·mol$^{-1}$) | $\Delta SE$ (kcal·mol$^{-1}$) | $\Delta$(Pt-Cl) (Å) |
| cisplatin | 2.37 | −0.115 | −0.014 | 5.6 | 7.6 | 0.01 |
| **1**-$PtCl_2(H_2O)$ | 1.22 | −0.112 | −0.015 | 4.4 | 6.4 | 0.00 |
| **2**-$PtCl_2(H_2O)$ | | | | | | |
| (*S,S*) | 4.21 | −0.016 | −0.072 | 3.9 | 5.9 | 0.005 |
| (*R,S*) | 11.77 | −0.088 | 0.111 | 4.3 | 6.1 | 0.01 |
| (*R,R*) | 12.01 | −0.076 | 0.123 | 5.9 | 8.0 | 0.01 |
| **3**-$PtCl_2(H_2O)$ | | | | | | |
| (*S,S*) | 4.43 | −0.028 | −0.076 | 4.0 | 6.0 | −0.005 |
| (*R,S*) | 11.10 | −0.071 | 0.166 | 4.9 | 6.8 | 0.00 |
| (*R,R*) | 8.39 | −0.060 | 0.125 | 6.4 | 8.4 | 0.00 |

[a] All *gauche* forms; *EH* energy of $H_2O$ was calculated and added to the *EH* values of the reactants; *MM* value of $H_2O$ was not possible to be calculated, the *MM* values of the reactants were not corrected

($\Delta SE \approx 6.0$ kcal·mol$^{-1}$) in agreement with experimental kinetic data. In terms of *EH* energy, however, the lowest barrier is provided by the **1**-$PtCl_2(H_2O)$ *gauche* conformer; this is in contrast with *MM* results and experimental data. For this reason, a comparison between the results for differently constituted compounds should be viewed with caution, and due respect should be given only to comparison among the different geometry isomers and conformers of one and the same compound. A more reliable method should be employed if comparison among the different compounds is desirable.

The energy values of both *MM* and *EH* point out that the (*S,S*) conformers offer the lowest energy change to attain the transition state. Although the absolute values do not inspire much credence (1–4 eV in terms of *EH*) for a reversible reaction (much higher than expected), the relative values do agree with experimental rate constants.

## Conclusions

The *cis*-$Pt(NH_3)_2Cl_2$ complex prefers a *trigonal bipyramid* transition state with NN at axial positions. The picture changes drastically when two $NH_3$ are substituted by an *en* ligand – the number of the possible isomers in reduced, and the *square pyramid* becomes the preferred arrangement with Cl at apical position. Location of an *en* ligand in equatorial position in a *trigonal bipyramid* becomes energetically very unfavourable due to the required high NPtN angle in such a position (120°); those structures are unrealistic giving preference to *square pyramid* structures with *en* taking two basal positions. With unsubstituted *en*, a *square pyramid* with Cl or O at the apical position offers the lowest energy hydrolysis path. In substituted *en* compounds (**2**-$PtCl_2(H_2O)$ and **3**-$PtCl_2(H_2O)$), the Pt-Cl basal distance is longer than the Pt-Cl apical one. Thus, it is expected that the release of the basal $Cl^-$ is facilitated, and a substituted *en* complex offers a lower energy mechanistic path

than an unsubstituted *en* or the cisplatin complex. *MM* results point out that – in agreement with experimental results – the hydrolysis reaction is faster for the (*S,S*) conformer as compared to that of the (*R,S*) conformer of the **3**-$PtCl_2$ compound. The calculated values of distortion vectors support and finalize the conclusions based on molecular mechanical optimized geometries: the least distorted geometry is a *trigonal bipyramid* for cisplatin and *square pyramid* for the analogues. The contributions of the bending modes to the deformation vector are predominant; those of the stretching modes for *square pyramid* and *trigonal bipyramid* are very small. This indicates that there are only small bond length variations (especially apical) – a result which has also been obtained by molecular mechanical calculations. The largest contribution to the *TBP* angular distortion comes from the $S_{6a}$ and $S_{6b}$ modes which suggests that there is much motion in the equatorial plane and less tilting of the axial bonds. Both for the *trigonal bipyramid* and for the *square pyramid,* the predominant distortions arise from modes which are involved in a *Berry* twist, although the contributions of other modes, especially the totally symmetric ones, are not negligible.

## Appendix

The *MMX* force field includes the following terms: bond stretch $E_r$, valence angle deformation $E_v$, cross-term for bond-angle interaction $E_{r-v}$, torsional energy $E_t$, *van der Waals* (non-bonded) interactions $E_{vdw}$, dipole-dipole interaction $E_{dd}$. Both $E_r$ and $E_v$ are treated by the *Hook* law. For details, see Ref. [19]. The set of parameters used in this investigation is given below.

| Stretch | $k_r$ (mdyn· ($Å^{-1}$) | | Standard bond length (Å) | | Bond moment (*D*) |
|---|---|---|---|---|---|
| | This work | Literature | This work | Literature | |
| Pt–LP | 2.000 | – | 0.800 | – | – |
| Pt–Cl | 2.000 | 1.47 [18] | 2.300 | 2.30 [18] | 0.000 |
| Pt–N | 2.000 | 2.54 [16b]<br>1.68 [18] | 1.980 | 2.03 [16b]<br>2.00 [18] | 0.000 |
| Pt–O | 2.000 | – | 1.800 | – | 0.000 |
| Pt–O | 2.000 | – | 1.800 | – | – |
| N–C | 5.100 | 6.00 [16c, 14c] | 1.440 | 1.49 [16c, 14c] | 0.040 |
| C–C | 4.400 | 5.00 [16c, 14c]<br>4.50 [18] | 1.523 | 1.50 [16c, 14c]<br>1.54 [18] | 0.000 |
| N–H | 6.100 | 5.64 [16c, 14c]<br>4.92 [18] | 1.015 | 0.91 [16c, 14c]<br>1.00 [18] | −0.760 |
| C–H | 4.600 | 5.00 [16c, 14c]<br>4.55 [18] | 1.113 | 0.97 [16c, 14c]<br>1.09 [18] | 0.000 |
| $C–C_{ar}$ | 5.000 | 5.00 [14c] | 1.497 | 1.50 [14c] | 0.000 |
| $C_{ar}–C_{ar}$ | 9.600 | – | 1.337 | – | 0.000 |
| $C_{ar}$–H | 4.600 | 5.00 [14c] | 1.101 | 0.97 [14c] | −0.200 |
| O–H | 4.600 | 5.00 [14c] | 0.942 | 0.91 [14c] | −1.115 |
| $C_{ar}$–O(H) | 6.800 | – | 1.355 | – | 0.000 |
| N–LP | 4.500 | – | 0.600 | – | 0.600 |
| O–LP | 4.500 | – | 0.600 | – | 0.900 |

| Bend | $k_\theta$(mdyn·Å$^{-1}$) | | Standard valence angle (°) | |
|---|---|---|---|---|
| | This work | Literature | This work | Literature |
| Cl–Pt–Cl | 0.000 | 0.000 [14c], 0.28 [16d-g] | 90, 120, 180 | 86.6 [16d-g] |
| Cl–Pt–N | 0.000 | 0.000 [14c], 0.28 [16d-g] | 90, 120, 180 | 86.6 [16d-g] |
| Cl–Pt–O | 0.000 | 0.000 [14c] | 90, 120, 180 | – |
| N–Pt-O | 0.000 | 0.000 [14c] | 90, 120, 180 | – |
| N–Pt–N | 0.000 | 0.000 [14c], 0.400 [16d-g] | 90, 120, 180 | 90.0 [16d-g] |
| Pt–N–C | 0.000 | 0.300 [16b], 0.280 [16d-g] | | 127.3 [16b], 110.0 [14c] |
| | | 0.200 [14c] | | 109.5 [16d-g] |
| Pt–O–H | 0.000 | 0.100 [14c] | | 109.7 [14c] |
| N–C–C | 0.570 | 0.500 [16c], 0.45 [14c] | 109.47 | – |
| N–C–$C_{ar}$ | 1.045 | – | 110.74 | – |
| C–C–$C_{ar}$ | 0.450 | – | 109.47 | – |
| C–$C_{ar}$–$C_{ar}$ | 0.550 | – | 121.40 | – |
| $C_{ar}$–$C_{ar}$–O | 0.700 | – | 124.30 | – |
| $C_{ar}$–$C_{ar}$–$C_{ar}$ | 0.430 | – | 120.00 | – |
| Pt–N–H | 0.000 | 0.100 [14c], 0.28 [16d-g] | 109.70 | 109.7 [14c], 109.5 [16d-g] |
| Pt–N–LP | 0.000 | – | | – |
| Pt–O–LP | 0.000 | – | | – |
| H–N–H | 0.500 | 0.320 [16c], 0.330 [14c] | 104.50 | 108.98 [14c] |
| H–N–C | 0.500 | 0.360 [16c], 0.450 [14c] | 109.47 | 109.49 [14c] |
| LP–N–C | 0.500 | – | 109.20 | – |
| N–C–H | 0.500 | 0.360 [16c], | 108.80 | 108.98 [16c] |
| H–C–H | 0.320 | 0.320 [16c], | 109.40 | 108.98 [16c] |
| C–C–H | 0.360 | 0.360 [16c, 14c] | 109.39 | 109.38 [14c] |
| | | 0.450 [14c] | | |
| $C_{ar}$–O–LP | 0.100 | – | 120.00 | – |
| LP–O–LP | 0.240 | – | 131.00 | – |
| LP–O–H | 0.240 | – | 101.01 | – |
| LP–N–H | 0.500 | – | 108.00 | – |

| Torsional (this work) | $V_1$ | $V_2$ | $V_3$ |
|---|---|---|---|
| N–C–C–N | −0.400 | −1.100 | 1.200 |
| N–C–$C_{ar}$–$C_{ar}$ | 0.000 | 0.000 | 0.000 |
| C–C–N–LP | 0.200 | −0.220 | 0.100 |
| $C_{ar}$–C–N–LP | 0.000 | 0.000 | 0.000 |

| *Van der Waals* | *R* | | *EPS* | | *LPD* | *IHTYP* |
|---|---|---|---|---|---|---|
| | This work | Literature | This work | Literature | | |
| C ($sp^3$) | 1.900 | 1.900 [14c] | 0.044 | 0.044 [14c] | 0 | 0 |
| C ($sp^2$) | 1.940 | – | 0.044 | – | 110 | 0 |
| H (C–H) | 1.500 | 1.440 [14c] | 0.047 | 0.024 [14c] | 0 | 20 |
| O (C–OH) | 1.740 | 1.700 [14c] | 0.050 | 0.055 [14c] | 90 | 0 |
| N ($sp^3$) | 1.820 | 1.800 [14c] | 0.055 | 0.050 [14c] | 200 | 0 |
| Cl | 2.030 | – | 0.240 | – | 10 | 0 |
| LP | 1.200 | – | 0.016 | – | 0 | 0 |
| $C_{ar}$ | 1.900 | – | 0.044 | – | 110 | 0 |

(continued)

| | | | | | | |
|---|---|---|---|---|---|---|
| H (OH) | 1.100 | – | 0.036 | – | 0 | 40 |
| H (NH) | 1.125 | – | 0.034 | – | 0 | 0 |
| $M_1$ | 0.000 | – | 0.400 | – | 0 | 0 |
| $M_2$ | 0.000 | – | 0.400 | – | 0 | 0 |
| $M_3$ | 0.000 | – | 0.400 | – | 0 | 0 |
| Spherical $H_2O$ | 1.530 | – | 0.500 | – | 0 | 0 |
| Out-of-plane bending (this work) | | | | | | |
| $C–C_{ar}$ | 0.800 | | | | | |
| $C_{ar}–C_{ar}$ | 0.800 | | | | | |
| C–O | 0.800 | | | | | |
| Stretch-bend (this work) | | | | | | |
| Stretch-bend (1) | 0.12 | | | | | |
| Stretch-bend (2) | 0.25 | | | | | |
| Stretch-bend (3) | 0.09 | | | | | |
| Stretch-bend (4) | -0.40 | | | | | |

For explanation of the abbreviations used in this Table, see Ref. [19]

## Acknowledgements

*N.T.* is grateful to the University of Regensburg (FRG) and the *German Science Foundation* (DFG) for providing financial support during her stay in FRG. Financial support by the *Bulgarian National Research Fund* through Grants 466 and 306 is also acknowledged. The authors are grateful to Dr. *H. H. Homeier* (University of Regensburg, FRG) for critically reading the manuscript.

## References

[1] Nikolov GSt, Trendafilova N, Schönenberger H, Gust R, Kritzenberger J, Yersin H (1994) Inorg Chim Acta **217:** 159

[2] Lepre CA, Lippard SJ (1990) In: Eckstein F, Lilley DMJ (eds) Nucleic Acids and Molecular Biology, vol. 4. Springer, Berlin Heidelberg and refs therein

[3] Lippert B (1989) Progr Inorg Chem **37:** 2; Umapathy P (1989) Coord Chem Revs **95:** 129

[4] Rosenberg B, Van Camp L, Krigas T (1965) Nature London **205:** 698

[5] Wappes B, Jennerwein M, Angerer EV, Schönenberger H, Engel J, Berger M, Wrobel K-H (1984) J Med Chem **27:** 1280

[6] Müller R, Gust R, Bernhard G, Keller C, Schönenberger H, Seeber S, Osieka R, Eastman A, Jennerwein M (1990) J Cancer Res Clin Oncol **116:** 237

[7] (a) Bernhardt G, Gust R, Reile H, von Orde H-D, Müller R, Keller C, Spruß T, Schönenberger H, Burgermeister T, Mannschreck A, Range K-J, Klement U (1992) J Cancer Res Clin Oncol **118:** 201; (b) Jennerwein M, Wappes B, Gust R, Schönenberger H, Engel J, Seeber S, Osieka R (1988) J Cancer Res Clin Oncol **114:** 347

[8] Jennerwein M, Gust R, Müller R, Schönenberger H, Engel J, Berger MR, Schmähl D, Seeber S, Osieka R, Atassi G, Maréchal-de Bock D (1989) Arch Pharm **322:** 67

[9] Kepert DL (1982) Inorganic Stereochemistry. Springer, Berlin, chapt 5

[10] (a) Burdett JK (1977) Inorg Chem **16:** 3013; Burdett JK (1980) Molecular Shapes. Wiley, New York; (b) Rossi AR, Hoffman R (1975) Inorg Chem **14:** 365; (c) Nikolov GSt (1994) Inorg Chem **33:** 1144

[11] Altona C, Faber DH (1974) Empirical Force-Field Calculations. A Tool in Structural Organic Chemistry. Topics Current Chemistry **45:** 1

[12] Field MJ, Bash PA, Karplus M (1990) Comput Chem **11:** 700
[13] Bersucker B, Leong MK, Boggs JE Pearlman RS (unpublished)
[14] (a) Comba P (1993) Coord Chem Revs **123:** 1 and refs therein; (b) Comba P, Zimmer M (1994) Inorg Chem **33:** 5368; (c) Bernhardt PV, Comba P (1992) Inorg Chem **31:** 2638; (d) Comba P (1994) Comments on Inorg Chem **16:** 3; (e) Zimmer M (1995) Chem Revs **95**: 2629
[15] Basch H, Krauss M, Stevens WJ, Cohen D (1985) Inorg Chem **24:** 3313
[16] (a) Hambley T W (1991) Inorg Chem **30:** 937; (b) Hambley TW (1988) Inorg Chem **27:** 1073; (c) Hambley TW, Hawkins CJ, Palmer JA, Snow MR (1981) Aust J Chem **34:** 45; (d) Snow MR (1970) JACS **92:** 3610; (e) Buckingham DA, Maxwell IE, Snow MR (1970) JACS **92:** 3617; (g) Gollogley JR, Hawkins CJ (1969) Inorg Chem **8:** 1168; (1970) **9:** 576
[17] MMX, *Q.C.P.E.* 395, Bloomington, IN, USA
[18] DeHayes LJ, Busch DH (1973) Inorg Chem **12:** 1505 and refs therein
[19] Clark T (1985) A Handbook of Computational Chemistry. Wiley, New York
[20] Boyens JCA (1985) Structure and Bonding **63:** 67
[21] Jensen F (1994) J Compt Chem **15:** 1199
[22] Calzaferri G, Forss L, Kamber I (1989) J Phys Chem **93:** 5366
[23] Fitzpatrick NJ, Murphy GH (1986) Inorg Chim Acta **111:** 139; (1984) Inorg Chim Acta **87:** 41
[24] (a) Jostes R (1988) Theor Chim Acta **74:** 229; (b) Baranovskii VI, Nikol'skii AV (1967) Teor Eksp Khim **3:** 527
[25] auf der Heyde TPE, Bürgi H-H (1989) Inorg Chem **28:** 3960, 3970, 3982
[26] Bevensee RM (1993) Maximum Entropy Solutions to Scientific Problems. Prentice Hall, Englewood Cliffs, NJ
[27] Hancock RD (1989) Progr Inorg Chem **37:** 187; (1992) J Chem Educ **69:** 615
[28] Gust R, Schönenberger H, Kritzenberger J, Range K-J, Klement U, Burgemeister T (1993) Inorg Chim **32:** 5939
[29] Berry RS (1960) J Chem Phys **32:** 933

*Received August 16, 1996. Accepted December 27, 1996*